HEAT TRANSFER CHARACTERISTICS OF WATER FLOW THROUGH A MICROTUBE

by

Cansın Balcı

Submitted to Graduate School of Natural and Applied Sciences
in Partial Fulfillment of the Requirements
for the Degree of Master of Science in
Mechanical Engineering

Yeditepe University
2023

HEAT TRANSFER CHARACTERISTICS OF WATER FLOW THROUGH A MICROTUBE

APPROVED BY:

Prof. Dr. Erdem An ....
(Thesis Supervisor)
(Yeditepe University)

Prof. Dr. Emre Alpman ....
(Marmara University)

Assoc. Prof. Dr. Ali Bahadır Olcay ....
(Yeditepe University)

DATE OF APPROVAL: ..../..../20..

I hereby declare that this thesis is my own work and that all information in this thesis has been obtained and presented in accordance with academic rules and ethical conduct. I have fully cited and referenced all material and results as required by these rules and conduct, and this thesis study does not contain any plagiarism. If any material used in the thesis requires copyright, the necessary permissions have been obtained. No material from this thesis has been used for the award of another degree.

I accept all kinds of legal liability that may arise in case contrary to these situations.

Name, Last name Cansın Balcı

Signature …..…………………….……………………..

ACKNOWLEDGEMENTS

I am grateful to my thesis adviser, Professor Erdem An (Hojin Ahn), for his mentorship, patience, and guidance on this project. His knowledge about experimental work and the lessons I attend at master progress will guide me through my carrier.

I want to thank my lab partner Aleyna Kiraz, for all the good times we had during the project.

Lastly, I would like to thank my family and friends for their support and motivation during this project.

ABSTRACT

HEAT TRANSFER CHARACTERISTICS OF WATER FLOW THROUGH A MICROTUBE

Convection heat transfer of vertically downward and horizontal flows was experimentally studied using a microtube, 0.501 and 1.00 mm in inner and outer diameters, respectively, and 398 mm in length. The test section was built in a vacuum chamber maintained approximately at the absolute pressure of 1 kPa. Tests used water as the working fluid with constant heat flux boundary conditions. Reynolds numbers at the tube inlet were between 600 and 2000, with heat fluxes varying from 3.5 to 87 kW/m^2. The wall temperatures were measured employing 17 T-type thermocouples, each embedded in a small solder cast attached to the microtube. Two extra thermocouples measured the environment temperature inside the vacuum chamber. At low heat flux, the Nusselt number converged to a range of 4.36 and 4.36 + 8%. However, as the heat flux increased to greater than 26 kW/m^2, the Nusselt number started deviating far above 4.36 due to the effect of mixed convection. No difference between vertical and horizontal configurations was observed in heat transfer rate at Reynolds numbers less than 1800 at the tube inlet for all heat fluxes. However, when the Reynolds number was larger than 2000 at the tube inlet, the Nusselt number of vertically downward flow was greater than that of horizontal flow. Furthermore, at the high Reynolds number, the heat transfer rate of the vertical flow monotonously increased toward the tube inlet while the horizontal flow appeared thermally fully developed.

ÖZET

MİKROTÜP İÇERİSİNDEKİ SU AKIŞININ ISI TRANSFER ÖZELLİKLERİ

Dikey olarak aşağı doğru ve yatay akışların konveksiyon ısı transferi, iç ve dış çapları sırasıyla 0.501 ve 1.00 mm ve uzunluğu 398 mm olan bir mikro tüp kullanılarak deneysel olarak incelenmiştir. Test bölümü, yaklaşık olarak 1 kPa'lık mutlak basınçta tutulan bir vakum odasında oluşturulmuştur. Testlerde çalışma sıvısı olarak su seçilip sabit ısı akısı sını koşulu kullanılmıştır. Tüp girişindeki Reynolds sayısı 600 ve 200 arasında, ısı akışları 3.5 ile 87 kW/m^2 arasında değişiyordu. Duvar sıcaklıkları 17 adet T-tipi termokupl kullanılarak ölçüldü, her biri küçük bir lehim kalıbına gömülüp mikro tüpe bağlanmıştır. İki ekstra termokupl, vakum odasının içindeki ortam sıcaklığını ölçtü. Düşük ısı akısında, Nusselt sayısı 4.36 ve 4.36 + %8 aralığına yakınsadı. Ancak ısı akısı 26 kW/m^2'nin üzerine çıktıkça, karışık konveksiyonun etkisiyle Nusselt sayısı 4.36'nın çok üzerinde sapmaya başladı. Tüm ısı akıları için boru girişindeki Reynolds sayısı 1800'den küçükken ısı transfer hızında dikey ve yatay konfigürasyonlar arasında fark gözlenmedi. Ancak, boru girişindeki Reynolds sayısı 2000'den büyük olduğunda, Nusselt sayısı dikey olarak aşağı doğru akışta yatay akıştan daha büyüktü. Ayrıca, yüksek Reynolds sayısında, dikey akışın ısı transfer hızı boru girişine doğru monoton bir şekilde artarken, yatay akış termal olarak tamamen gelişmiş görünmektedir.

TABLE OF CONTENTS

LIST OF FIGURES

LIST OF TABLES

LIST OF SYMBOLS/ABBREVIATIONS

$\dot{m}$	Mass flow rate (kg/sn)
A	Area (m^2)
A_{cross}	Cross-section area (m^2)
d_i	Inner diameter (m)
d_o	Outer diameter (m)
h_i	Enthalpy (kJ/kg)
h_{loss}	Heat loss coefficient ($W/m^2 \cdot K$)
htc	Heat transfer coefficient ($W/m^2 \cdot K$)
I	Current (A)
k	Thermal conductivity ($W/m \cdot K$)
L	Length (m)
L_{heated}	Heated length (m)
Q	Heat transfer rate (W)
q''	Heat flux (W/m^2)
q_{con}	Conduction heat flux (W/m^2)
q_{gen}	Heat generation (W/m^2)
q_{net}	Net heat flux (W/m^2)
R	Resistance (Ω)
$T_{ambient}$	Ambient temperature (°C)
T_{wall}	Wall temperature (°C)
$T_{wall,i}$	Inner wall temperature (°C)

$T_{wall,o}$	Outer wall temperature (°C)
V	Voltage (V)

Greek symbols

α	Kinetic energy correction factor
μ	Dynamic viscosity (Pa·s)
ν	Kinematic viscosity (m^2/s)
ρ	Density (kg/m^3)

Dimensionless numbers

Gz	Graetz number
Nu	Nusselt number
Pr	Prandtl number
Re	Reynolds number

1. INTRODUCTION

Heat transfer characteristics of water flow have been extensively investigated in large and long pipes. However, there is little research on heat transfer characteristics in microtubes with diameters less than 1 mm. Due to technological advancements, small devices and systems must be cooled or heated.

Most of the existing correlations in the literature were obtained for large pipes. However, convective heat transfer rate and radiation heat transfer increase when the diameter of the tube decrease in the laminar flow.

The conventional correlations consider fluid characteristics such as density and viscosity constant. However, in reality, properties change through microtube. Thus, for the above reasons, correlations in the literature may not apply to microtubes.

Also, the effect of the configuration on the heat transfer has not been investigated. In most of the studies done for horizontal configuration, there is a lack of study in vertical configuration. Therefore, this search's scope is to investigate the heat transfer characteristics of laminar water flow in the microtube with horizontal and vertical configurations.

Convection heat transfer is classified as free convection and forced convection. In forced convection, fluid is forced to go through a tube by an external force such as a pump. On the other hand, there is no external effect in natural convection. For example, the microtube wall is heated under the constant heat flux boundary condition, and near the microtube wall air density gets lower and lighter air goes up.

Reynolds number is a dimensionless number used to characterize the flow type. Flow is considered as laminar until Reynolds around 2300, between Reynolds 2300 to 4000 flow named by translation flow, and when Reynolds greater than 4000, flow type is defined as turbulent.

Nusselt number is the ratio of convective and conductive heat transfer. Thus this dimensionless number is investigated in heat transfer experiments. Nusselt number considered 4.36 for constant heat flux boundary condition in fully developed flow.

The inverse Graetz number is another dimensionless number used to characterize the flow. Flow is considered as fully developed for greater values of 0.05 inverse Graetz number. Dimensionless numbers were demonstrated in the data reduction part.

Thermocouples are very commonly used sensors in temperature measurements. Two-wired thermocouples include two different materials. When the thermocouple is heated or cooled, a voltage accurses, and the temperature is calculated from this voltage. In our study, T-type thermocouples were used for temperature measurements, and one four-wired, highly accurate thermocouple called PT100 was used for calibration.

2. LITERATURE SURVEY

Heat transfer characteristics of water flow have been extensively investigated in large and long pipes. For instance, in the article by Meyer et al. [1], a copper tube with an inner diameter of 11.5 mm and a length of 9.81 and a 316L stainless steel tube with an inner diameter of 4 mm and a length of 6m was used.

Thermocouples are often used for temperature measurements in heat transfer experiments. Electrical insulation and contact resistance should be considered before the thermocouple attachment process. In the study of Meyer et al. [1], a copper tube with an inner diameter of 11.5 mm was drilled with a 0.3 mm indentation, and a thermocouple was soldered in that indentation. 316L stainless steel tube with an inner diameter of 4 mm was drilled 0.5 mm, and a thermocouple was glued in the indentation using thermal adhesive (thermal conductivity k = 9 W/m·K for thermal adhesive). Kapton film was used for electrical insulation purposes. However, drilling indentations may be impossible since microtubes have small wall thicknesses. Celata et al. [2] attached K-type thermocouples on a microtube using cyanoacrylate adhesive and then fixed them with epoxy resin. However, since epoxy resin cannot be removed easily, any changes in thermocouple positions could not be possible. Öztabak et al. [3] developed a new method for thermocouple attachment. A small piece of solder was shaped by a mold assembly. The tip of the thermocouple was embedded in a solder cast. The solder cast covers half of the microtube, and thus, the contact area increased. Thermal paste was applied between the microtube and the solder cast to ensure electrical insulation. Lin and Yang [4] used the liquid crystal method (LCT) in their studies to measure the microtube wall temperature.

In literature, the Nusselt number for laminar flow converges to 4.36 under the constant heat flux boundary condition. This theoretical value is obtained assuming no property change. But in reality, properties change, and the Nusselt number increases in mixed convection. It is challenging to obtain forced convection conditions in the experiments. In order to study forced convection, the heat flux applied to the microtube must be low [1]. Thus, the difference between the microtube wall and fluid temperatures is slight. In Meyer and Evert's [1] study, the average fully developed Nusselt number for a 4 mm inner diameter microtube with forced convection condition was 4.75, 8.9% more than the theoretical value of 4.36.

Lelea et al. [5] studied the heat transfer of microtubes with three different inner diameters. Microtube diameters were 0.1, 0.3, and 0.5 mm. A small amount of power was applied to the microtube to ensure forced convection. K-type thermocouples were placed on the microtubes, and all the experiments were conducted in a vacuum environment. Thermal uncertainty was calculated to reduce the uncertainties caused by heat losses from thermocouples. Thermal uncertainty was calculated by electrical input power and heat transferred to the water. Acceptable heat input values were obtained from the results of this calculation. Heat transfer results were consistent with the theoretical value of Nusselt number 4.36.

Yang and Lin [6] studied the heat transfer coefficient for six different microtubes with inner diameters of 123 μm, 220 μm, 308 μm, 416 μm, 764 μm, and 962 μm. Inner diameters were measured with a scanning electron microscope (123 μm to 416 μm) and an optical microscope (764 μm and 962 μm). The LCT method was used for measuring microtube wall temperature. The experiment results show that common correlations were available for heat transfer of fully developed flow in microtubes. However, in microtubes, the laminar thermal entry length was longer than established correlations. Although in most of the literature coefficient for thermal entry length is 0.05, Meyer et al. [1] suggested that the coefficient must be at least 0.12.

Zhuo Li et al. [7] conducted an experiment to investigate laminar flow heat transfer characteristics, and the results were compared with numerical solutions. The bulk temperature was calculated from experiments as well as numerical simulation and linear interpolation between the inlet and outlet. The effect of these three different calculation methods on the Nusselt number was examined. Heat transfer results are consistent with the literature, while the Reynolds number exceeds 100. Experimental results become biased from the literature as the wall-thickness-over-hydraulic diameter value increase while the Reynolds number is less than 100.

The article written by Celata et al. [2] gives information about the scaling effect on single-phase laminar flow with constant heat flux boundary condition in microtubes. Celata et al. indicate that local Nusselt numbers become less axis-depended while diameter decreases. However, smaller microtubes have a high length-to-diameter ratio. Thus, the flow may not become thermally developed.

Baek et al. [8] developed a method for laminar flow heat transfer coefficient calculations for microtubes (with non-negligible axial conduction) that are too small for thermocouple attachment. Constant Nusselt number values for Reynolds numbers between 300 and 2000 can be observed.

An article written by Meyer et al. [9] compares the flow regime maps with the experimental results. Flow maps in the literature become invalid for low Prandtl numbers values and small tube diameters. The flow maps developed by Meyer et al. have an extensive range of Prandtl numbers and tube diameters, and most of the maps also can be used in developing flow. Ghajar and Tang [10] studied flow maps and visualization for air-water two-phase flow for slightly increased pipes.

The effect of inclination on heat transfer for circular ducts was studied by Barozzi et al. [11]. Increasing the slope from 0 deg to 60 deg has a negligible effect on the heat transfer ratio.

Rosa et al. [12] reviewed articles written about heat transfer in microchannels and gave an excellent aspect for scaling effects in microchannels. It is suggested that, once the geometry of the cross-section, which scaling effects cannot be negligible and uncertainties of the experiment are decided, conventional correlations can be applied. Otherwise, results can be unreliable. Maranzana et al. [13] especially study axial conduction in mini and microchannels and propose a non-dimensional number M which was developed by considering the axial conduction effect. Their study shows that axial conduction becomes negligible when $M<10^{-2}$.

In the article by Mala and Li [14], water flow characteristics were studied in the silica and stainless steel microtubes. They observed early translation to turbulent and attributed this early translation to surface roughness.

3. EXPERIMENTAL METHOD

3.1. TEST SETUP

The layout of the experimental setup is shown in Fig 3.1. The experimental setup includes a compressor, an air tank, a water tank, a vacuum pump, two power supplies, a multimeter, an electronic balance, a DAQ, two pressure sensors, and a test section.

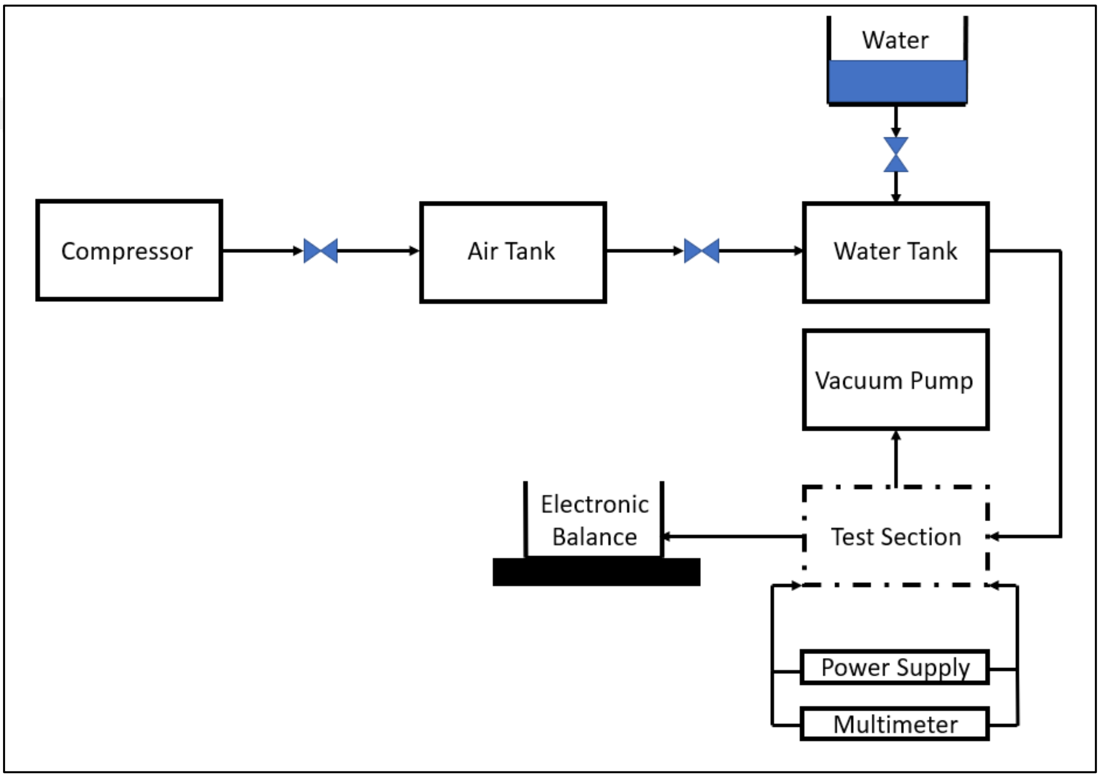

Figure 3.1. Schematic representation of the experimental setup

The air tank was filled with air by using the compressor until the desired pressure was reached. Within this process, we provided the desired pressure value to the water tank and set the Reynolds number required for the experiment. Experiments were conducted in a vacuum environment in order to prevent heat losses. VP2200N 2-stage vacuum pump was used for removing air from the test section. The power source provides a constant heat flux through the microtube. The second one provides power for a 4-20 mA pressure sensor and vacuum sensor. Details of the setup will be discussed in the following chapters.

Figure 3.2. (a) 3D CAD design, (b) manufactured design

The experiment setup was designed in the CAD program called Onshape and built at the Yeditepe University laboratory (Figure 3.2).

Manufactured parts can be seen in more detail in Figure 3.3. Microtube was placed between two brass parts, (a) and (b). Pressurized water enters the test section through the straight adapter (c) and goes to the elbow adapter (d). Elbow adapter placed on top brass part (a). And thus, the pressurized water reaches the microtube.

Three stud bolts (g) were used in order to connect the upper and lower parts of the setup. Different microtubes can be placed in this setup since the stud bolt height can be adjusted.

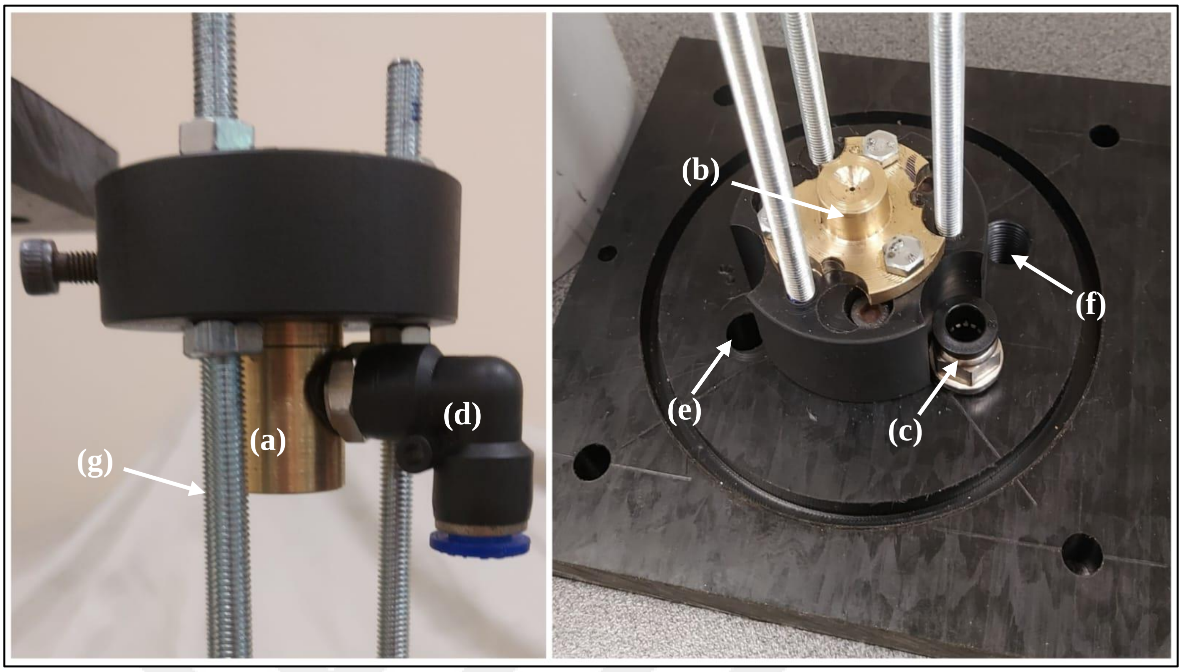

Figure 3.3. (a) Top brass, (b) Bottom brass, (c) Straight adapter, (d) Elbow adapter, (e) Hole for vacuum pump, (f) Hole for vacuum sensor, (g) Stud bolts

There are many ways for thermocouple attachment. Accurate temperature readings are mostly related to how thermocouples are attached to the microtube. Therefore, thermocouple attachment will be discussed in a separate section with more detail.

Table 3.1. Inner diameter, outer diameter, voltage length, heated length, and total length of the microtube

Inner diameter d_i [mm]	**Outer diameter do [mm]**	**Voltage length L_{volt} [mm]**	**Heated length L_{heat} [mm]**	**Total length L_{total} [mm]**
0.501	1.00	357	363	398

Electrical cables are soldered top and bottom brass parts, and voltage cables are soldered on the microtube as shown in Figure 3.4.

Figure 3.4. Electrical and voltage cables attachment

Figure 3.5. shows the devices used in the experiment. (a) ADC 3050DD power supply powering two 4-20 mA pressure transmitters. (d) The DCS10-120E power supply connected the brass parts as shown in Figure 3.4. and ensures the constant heat flux boundary condition for the microtube. Current readings were obtained by (b) 34461A Digital Multimeter, and temperature and voltage readings were obtained by (c) 34972A LXI Data Acquisition/Switch Unit (DAQ).

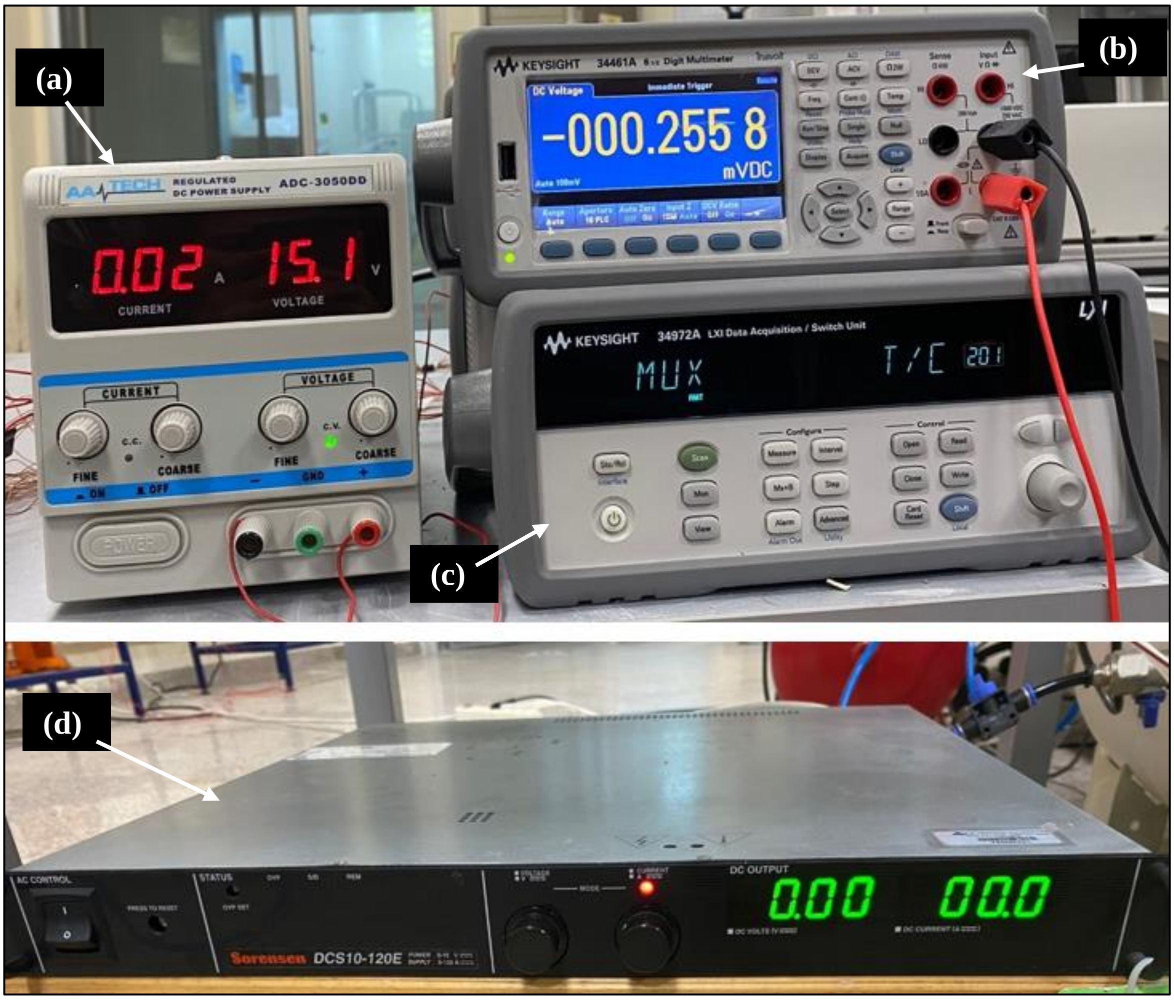

Figure 3.5. Devices used in the experiment setup. (a) ADC 3050DD power supply, (b) 34461A digital multimeter, (c) 34972A LXI data acquisition/switch unit, (d) DCS10-120E power supply

3.2. THERMOCOUPLE ATTACHMENT

Thermocouples were attached to the microtube, as shown in Figure 3.6. 17 T-type thermocouples were attached to the microtube, and two thermocouples got environment temperature readings.

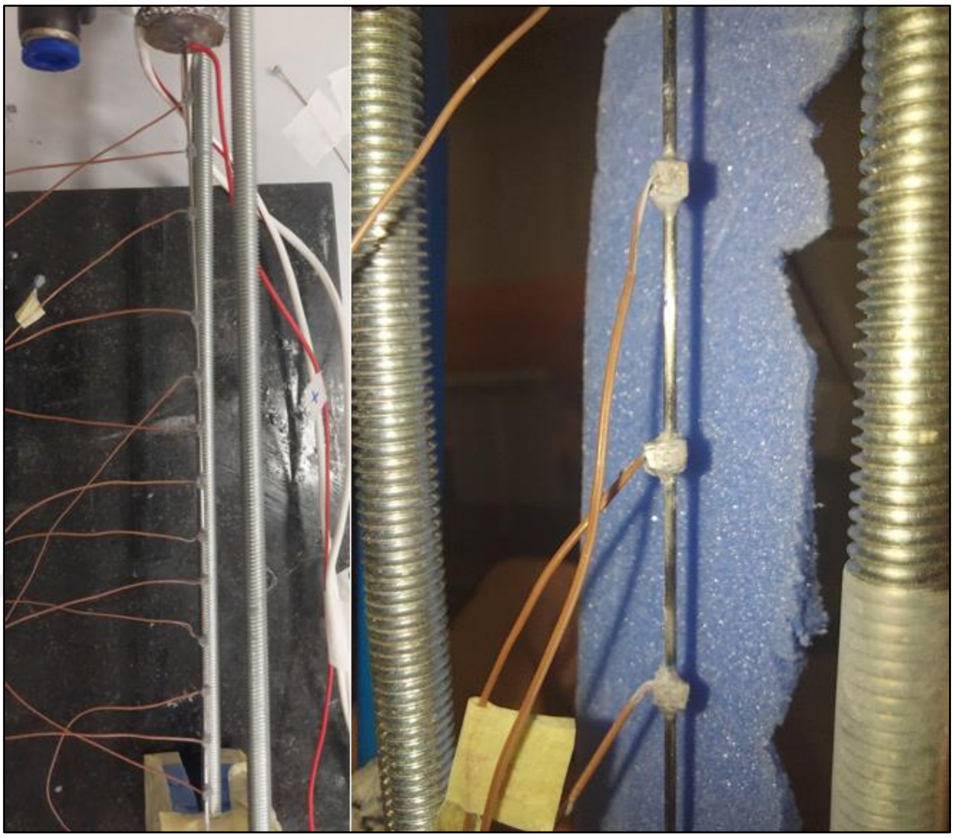

Figure 3.6. Thermocouples attached to the microtube

The solder cast method was used for thermocouple attachment. Solder casts cover the upper half of the microtube. Due to the large contact area and thermal paste applied between the thermocouple and microtube, the thermal contact resistance was reduced. [3]

A sufficient amount of thermal paste was applied on top of the microtube. Thermal paste provides electrical insulation between the microtube and solder cast. Thermal paste also removes all gasses; therefore, it prevents contact resistance. Thermal paste conductivity is k = 8.5 W/m·K.

Thermocouple was cautiously placed on the thermal paste. If too much pressure is applied on the solder cast while fixing, the thermal paste may overflow onto the pipe, and this cause a problem in electrical insulation.

After carefully placing the solder cast on top of the thermal paste, an instant adhesive was applied on both sides. The correct amount of instant adhesive should be used to avoid errors in temperature readings. After the thermocouple attachment is complete, thermocouple isolation must be checked by using a multimeter.

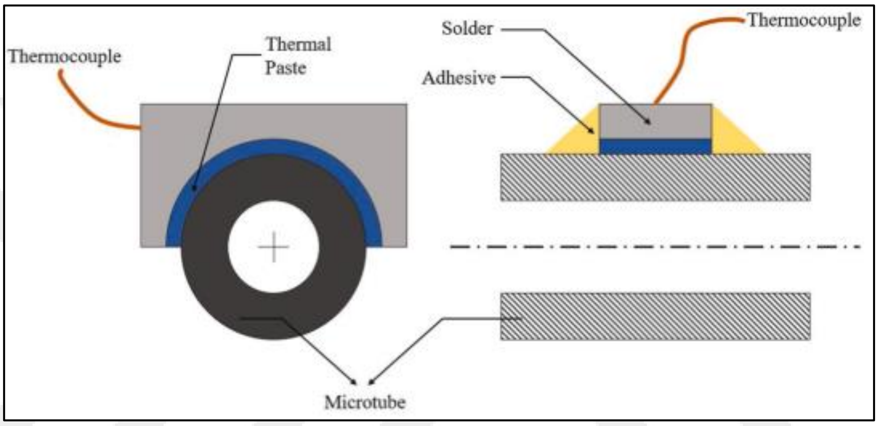

Figure 3.7. Detailed view of the attachment process of a thermocouple [3]

3.3. DIAMETER CALIBRATION

Before starting the experiment, it is necessary to ensure the inner diameter of the microtube. In this project, an experiment was used for the calculation of the inner diameter of the microtube.

Figure 3.8 demonstrates the experimental setup for diameter calibration. Microtube was attached to the tip of the water tank, and the electronic balance was used for mass readings.

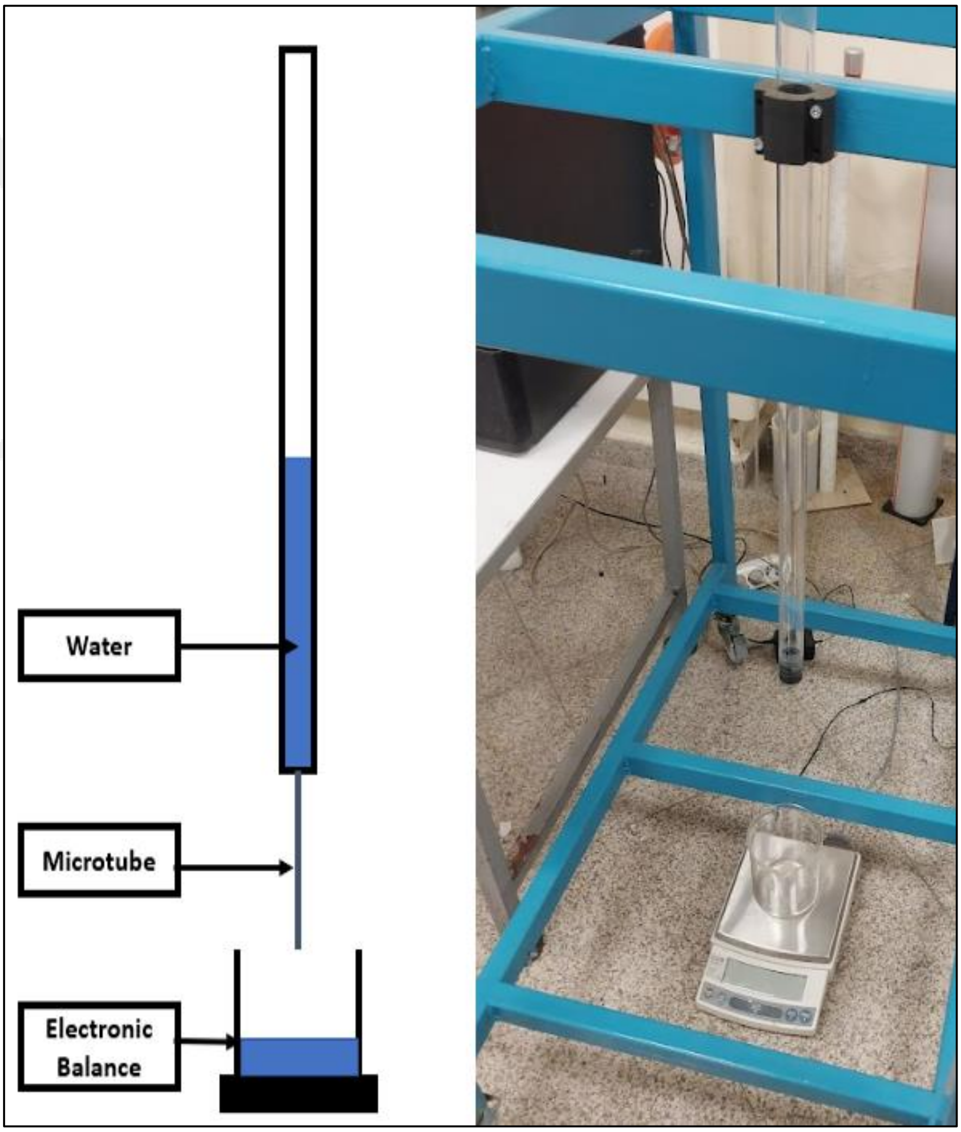

Figure 3.8. Experimental setup for diameter calibration

Inner diameter calculated from extended Bernoulli equation;

$$\left(\frac{P_1}{\rho g}+\alpha_1\frac{V_1^2}{2g}+z_1\right)-\left(\frac{P_2}{\rho g}+\alpha_2\frac{V_2^2}{2g}+z_2\right)=h_L \tag{3.1}$$

h_L is the head loss and α is the kinetic energy correction factor. After combining equation (3.1) with h_L and making the arrangements equation can be solved for tube diameter;

$$d=\left(\frac{\frac{128\mu L\dot{m}}{\rho\pi}+(\alpha_2+K_{ent})\frac{8\dot{m}^2}{\rho\pi^2}}{\rho g(H_t+L)}\right)^{1/4} \tag{3.2}$$

The mass flow rate is calculated from mass readings, and all the other values are known. The inner diameter of the microtube can be calculated. This experiment was done five times to make sure of the results.

3.4. THERMOCOUPLE CALIBRATION

The results of this experiment substantially depend on how accurate of the temperature readings are. However, since every thermocouple has different accuracy, some can read 0.4 °C more some can read 0.6 °C less. Thus, thermocouples were calibrated with the use of the high-accuracy four-wired thermocouple PT100. After the calibration is done, no changes should be made on the DAQ card. For instance, calibration is no longer valid if a voltage cable or thermocouple is removed from the DAQ card, and the whole calibration process should be redone. Figure 3.9 clearly shows the difference between calibrated data and the measured data.

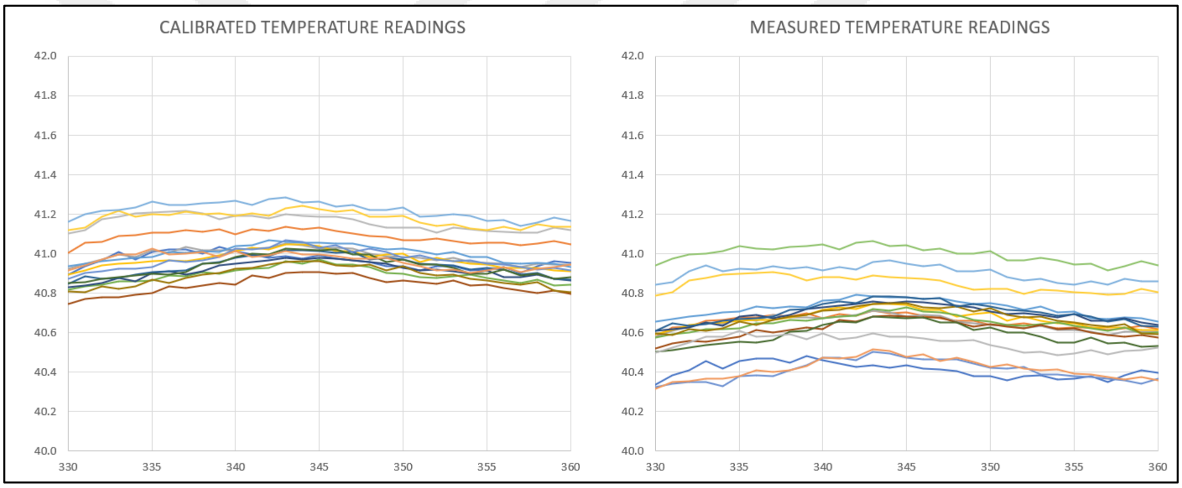

Figure 3.9. Calibrated temperature readings and Measured temperature readings

Thermocouples were placed around PT100 and tightened with electrical tape. It is essential to place thermocouples at the same height. Thermocouples are fixed with two stud bolts, as shown in Figure 3.10.

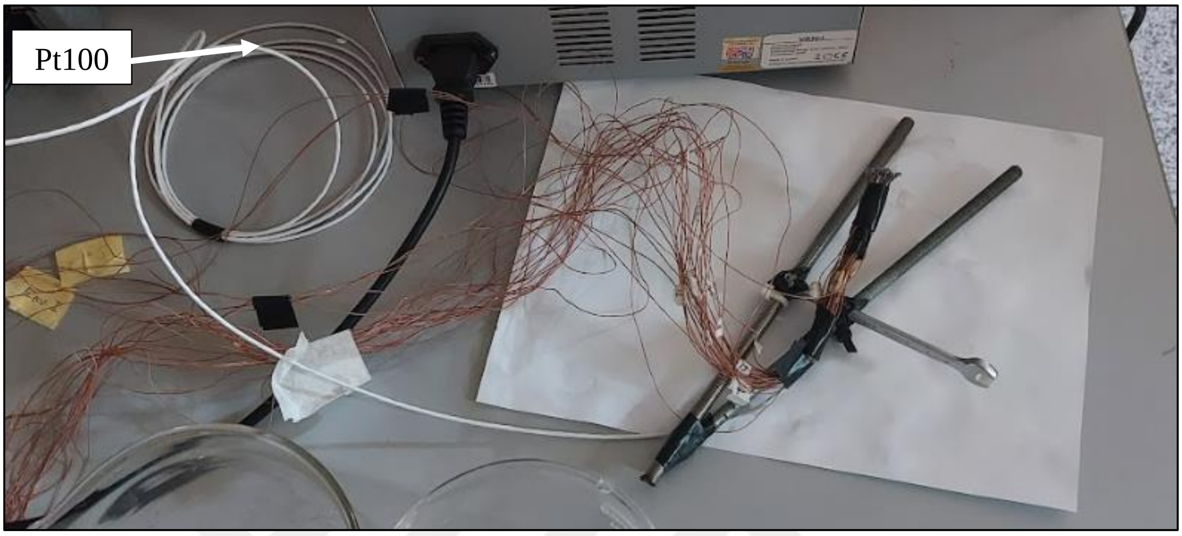

Figure 3.10. Thermocouple preparation for calibration progress

Thermocouples were placed in the beaker after the preparations of the thermocouples were completed. The water temperature gradually decreased from 90 °C to room temperature. A power source connected to the beaker was used to satisfy steady-state conditions with desired temperature intervals. Steady-state conditions were ensured every 10 °C.

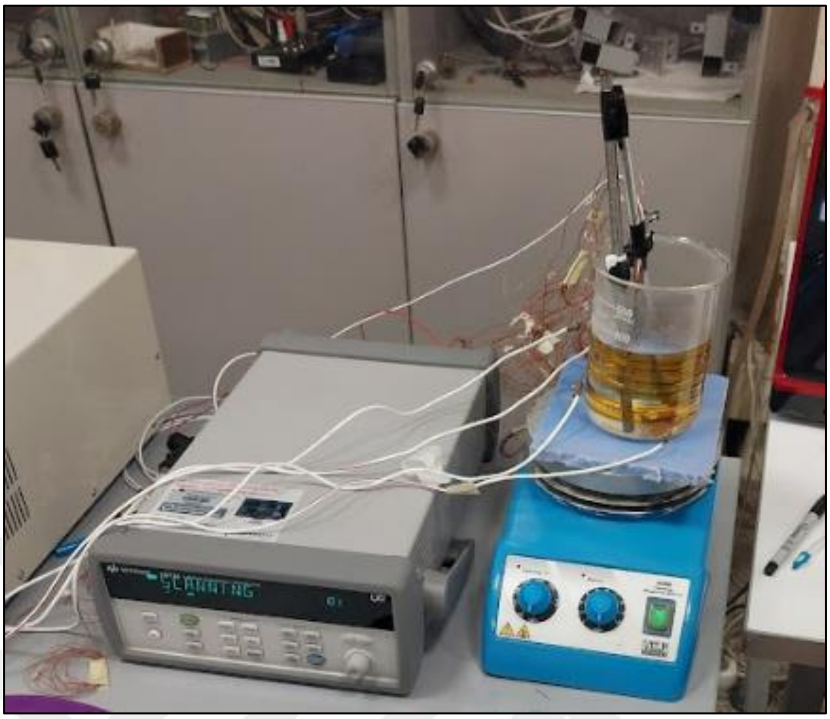

Figure 3.11. Test setup for thermocouple calibration

The temperature difference between every thermocouple and the PT100 was calculated at each steady-state interval. Calibration curves were obtained due to the difference between thermocouples and PT100. For instance, the calibration curve of TC101 was demonstrated in Figure 3.12.

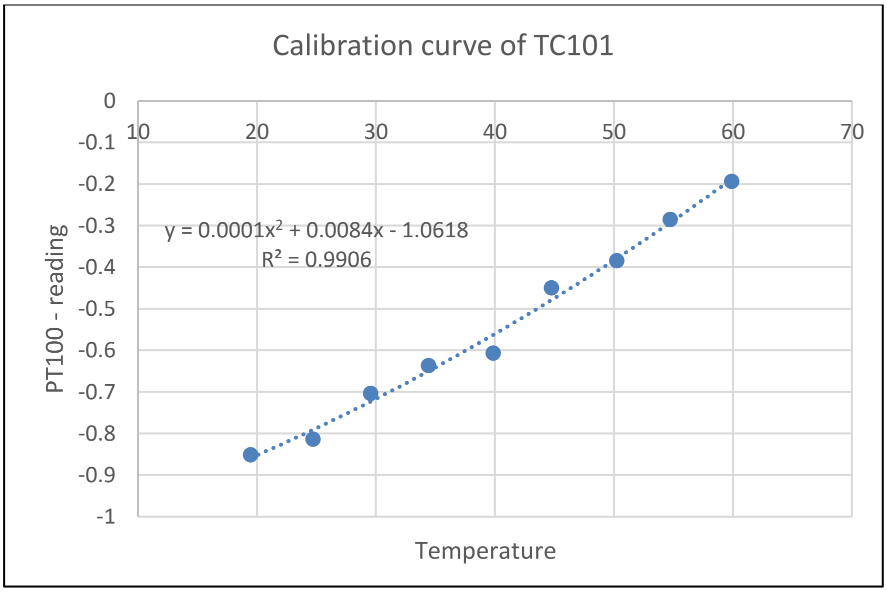

Figure 3.12. Calibration curve of TC101

Table 3.2. Equations obtained for thermocouple calibration.

Thermocouple Number	**Equation**
101	1,026E-04x2 + 8,434E-03x - 1,062E+00
104	2,701E-04x2 - 5,989E-03x - 6,306E-01
106	1,595E-04x2 + 1,872E-03x - 6,824E-01
109	2,461E-04x2 - 6,114E-03x - 4,367E-01
110	1,820E-04x2 - 1,021E-03x - 5,006E-01
111	2,084E-04x2 - 3,795E-03x - 4,124E-01
112	2,517E-04x2 - 7,293E-03x - 3,423E-01
113	1,735E-04x2 - 2,760E-03x - 3,845E-01
114	1,367E-04x2 + 1,180E-03x - 4,717E-01
115	7,235E-05x2 + 7,688E-03x - 6,446E-01
116	1,866E-04x2 - 1,431E-03x - 4,863E-01
118	2,250E-04x2 - 5,562E-03x - 4,896E-01
120	2,305E-04x2 - 3,378E-03x - 7,951E-01
201	2,817E-04x2 - 6,790E-03x - 6,050E-01
202	2,927E-04x2 - 8,074E-03x - 4,698E-01
203	2,972E-04x2 - 9,781E-03x - 3,732E-01
205	2,300E-04x2 - 4,376E-03x - 4,293E-01
206	2,697E-04x2 - 5,827E-03x - 3,429E-01
207	3,557E-04x2 - 1,373E-02x - 1,206E-01

3.5. DATA REDUCTION

Temperature values change alongside with the tube length. Therefore, water properties like viscosity cannot be assumed constant. Water properties were obtained from software called NIST, and equations for properties were created by the curve-fitting method. Calculations were done using the programming language called FORTRAN.

Reynolds number calculated as eq. (3.3). $\dot{m}$ is mass flow rate, d_o is the outer diameter, d_i is the inner diameter, μ is the dynamic viscosity.

$$Re = \frac{4\dot{m}d_o}{\pi\mu d_i} \tag{3.3}$$

In order to obtain free convection heat loss, an experiment was conducted, and the resistance value was calculated as follows.

$$R = \frac{\rho L_{heated}}{A_{cross}} \tag{3.4}$$

Temperature, current and voltage values were obtained from the conducted experiment for desired intervals.

$$Q = I^2 R \tag{3.5}$$

$$q'' = \frac{Q}{A} \tag{3.6}$$

The energy transfer rate and heat flux were calculated as (3.5) and (3.6), respectfully.

$$q'' = h_{loss}(T_{wall,o} - T_{ambient}) \tag{3.7}$$

$$h_{loss} = \frac{q''}{T_{wall,o} - T_{ambient}} \tag{3.8}$$

Heat loss coefficients (3.8) were evaluated by using the convective heat transfer formula (3.7) (Newton's law of cooling) and heat flux (3.6). $T_{wall,o}$ is the wall temperature of the microtube, and $T_{ambient}$ is the surrounding air temperature.

The energy balance for a small control volume was demonstrated in Figure 3.13. Axial conduction may count as negligible in large pipes, but neglecting it could be inaccurate on the microscale. Constant heat flux boundary condition was applied on the microtube. Therefore, there will be heat generation in the volume. Net heat flux q_{net} presented at eq. (3.9). q_{gen} is heat generation, q_{loss} is the heat losses from the microtube, and q_{cond} is the axial conduction.

$$q_{net} = q_{gen} - q_{loss} + q_{cond} \tag{3.9}$$

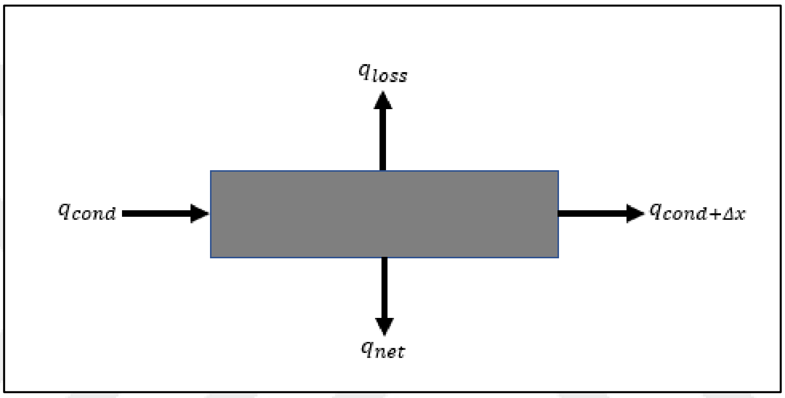

Figure 3.13. Energy balance of control volume

$$q_{gen} = \frac{\rho I^2}{A_{cross} \pi d_i} \tag{3.10}$$

Heat generation per unit volume found as eq. (3.9). ρ is the resistivity, I is current, and A_{cross} is the cross-sectional area.

q_{loss} calculates as follows;

$$q_{loss} = h_{loss} A (T_{wall} - T_{ambient}) \tag{3.11}$$

Axial conduction obtained from eq. (3.12). And integrated through a microtube.

$$q_{cond} = \left(-k A_{cross} \frac{dT}{dx}\right) \tag{3.12}$$

In order to obtain mean temperature, first fluid enthalpy *h* was calculated by integrating the net heat flux between thermocouple locations *i*. Meant temperature was obtained from NIST due to enthalpy values.

$$h_i = h_{i-1} + \frac{1}{\dot{m}} \int_i^{i+1} q_{net}\, dx \tag{3.13}$$

Surface temperatures $T_{wall,o}$ were obtained from thermocouples placed on the microtube to decide the inner wall temperature $T_{wall,i}$ one-dimensional conduction equation used as (3.14).

$$T_{wall,i} = T_{wall,o} - \frac{\dot{q} d_o^2}{16k}\left[2ln\frac{d_o}{d_i} - 1 + \left(\frac{d_i}{d_o}\right)^2\right] \tag{3.14}$$

After that net heat lux q_{net}, inner wall temperature $T_{wall,i}$ and mean temperature T_{mean} evaluated heat transfer coefficient htc was found as eq. (3.15).

$$htc = \frac{q_{net}}{T_{wall,i} - T_{mean}} \tag{3.15}$$

Mean Nusselt Nu_{mean}, Nusselt film Nu_{film} and inverse Graetz number calculated as follows;

$$Nu_{mean} = \frac{htcd_i}{k_{mean}} \tag{3.16}$$

$$Nu_{film} = \frac{htcd_i}{k_{film}} \tag{3.17}$$

$$Gz^{-1} = \frac{L_x}{d}\frac{1}{Re.Pr} \tag{3.18}$$

3.6. UNCERTAINTY ANALYSIS

The uncertainty of each experiment parameter was calculated with a 95% confidence level. The results of the analysis are represented in Table 3.3. Uncertainties in temperature measurements are the most significant uncertainty affecting the results. For example, the mean and wall temperature differences are around 0.6-0.7 °C when the heat flux is around 3.5 kW/m^2. The effect of uncertainties in temperature measurement on the Nusselt number is 20%.

Table 3.3. Uncertainty of experimental parameters

Parameters	**Uncertainty**
Temperature measurements	±0.154 °C
Mass flow rate	±0.97%
Resistivity	±0.65%
Heat loss coefficient	±1.2%
The inner diameter of the microtube	±0.25%

4. RESULTS

Experiments were conducted with respect to vertical downward and horizontal configurations, up to the initial Reynolds 2000 with varying seven different heat fluxes. The results of the experiments were compared with theoretical values.

4.1. VERTICAL DOWNWARD RESULTS

Heat fluxes of 3.5, 6.8, 10, 13.8, 26.8, and 56 kW/m^2 were applied on the microtube as constant heat flux boundary conditions. As the heat flux increases, the wall temperature of the microtube also increases from the beginning to the end of the tube. Thus, the Reynolds number also increases. This increase is demonstrated in Table 4.1. and as expected, the variation of the Reynolds number from the beginning to the end of the microtube was observed at most at 87 kW/m^2 heat flux value.

Table 4.1. Variation of Reynolds number at different currents along the pipe in vertical downward configuration

Reynolds number at the tube inlet	**3.5 [kW/m^2]**	**6.8 [kW/m^2]**	**10 [kW/m^2]**	**13.8 [kW/m^2]**	**26.8 [kW/m^2]**	**55.7 [kW/m^2]**	**87 [kW/m^2]**
600	600-627	617-669	633-711	651-757	709-920	818-1283	907-1655
767	767-794	787-838	805-881	824-929	888-1101	1000-1447	1097-1822
1068	1068-1097	1086-1136	1104-1181	1126-1233	1196-1407	1312-1755	1411-2125
1191	1191-1219	1205-1257	1218-1293	1240-1347	1307-1513	1419-1856	-
1460	1460-1486	1480-1530	1497-1571	1517-1621	1584-1790	1706-2145	1807-2516
1672	1672-1700	1695-1745	1714-1790	1730-1831	1798-2002	1918-2352	2006-2699
1943	1943-1971	1962-2014	1979-2052	1998-2101	2061-2266	2022-2460	2023-2722

The flow becomes fully developed in literature when the inverse Graetz number is greater than 0.05 for constant heat flux boundary condition. The blue line represents 0.05 the literature value of the inverse Graetz number and the red line represents the literature value of 4.36 of the Nusselt number in Figure 4.1. As is seen in Figure 4.1, some of the test results converge to the literature value of 4.36. Since water properties mainly depend on temperature, this convergence was valid in tests with low heat flux.

It is challenging to observe forced convection heat transfer. Forced convection can be observed only in low heat flux values. However, the wall and mean temperature difference are small in these heat flux values. Therefore, most of the existing data in the literature include a lot of uncertainties. For example, in Figure 4.2, wall temperature and mean temperature comparison are demonstrated for Reynolds at the tube inlet 1943 under the 3.5 kW/m^2 heat flux boundary condition. The mean and the wall temperature difference is 0.6-0.7 °C with ±0.15 °C uncertainty; this causes 22% uncertainty in the Nusselt number value. The difference between wall and mean temperatures increases as the heat flux value increases. (Figure 4.3-4.4)

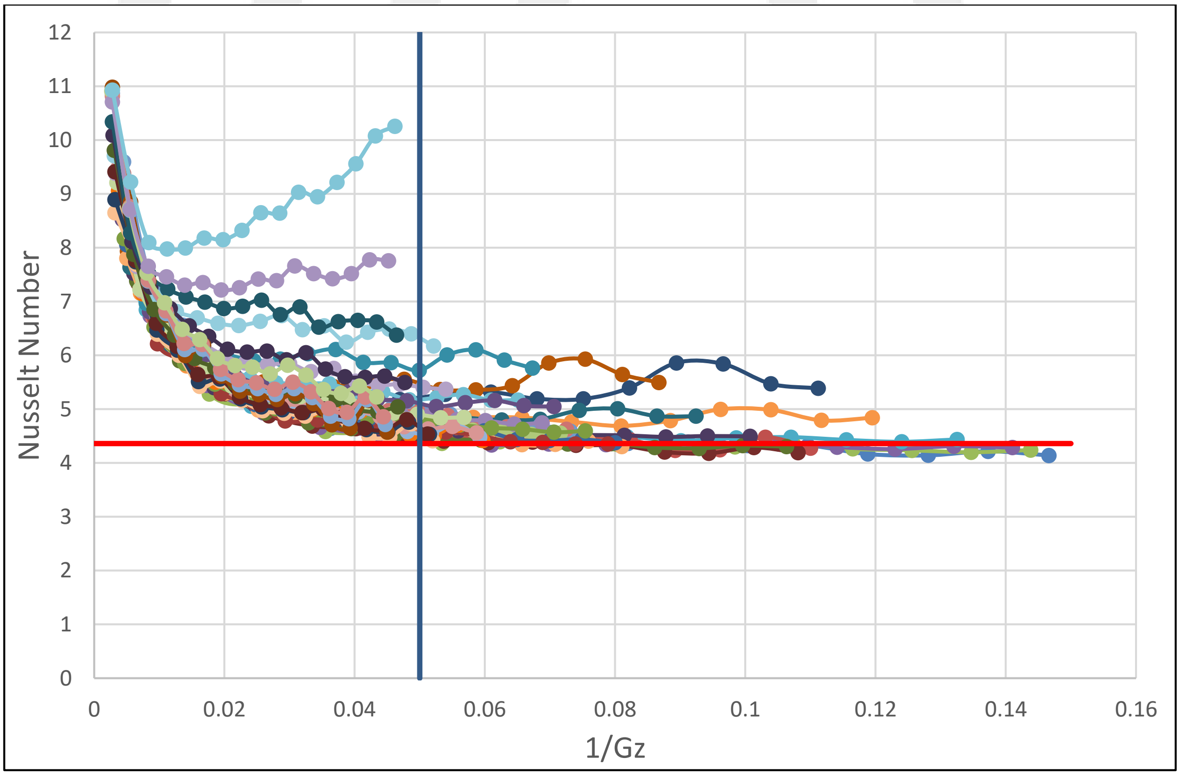

Figure 4.1. Vertically downward experiment results in heat fluxes of 3.5, 6.8, 10, 13.8, 26.8, 56, and 87 kW/m^2.

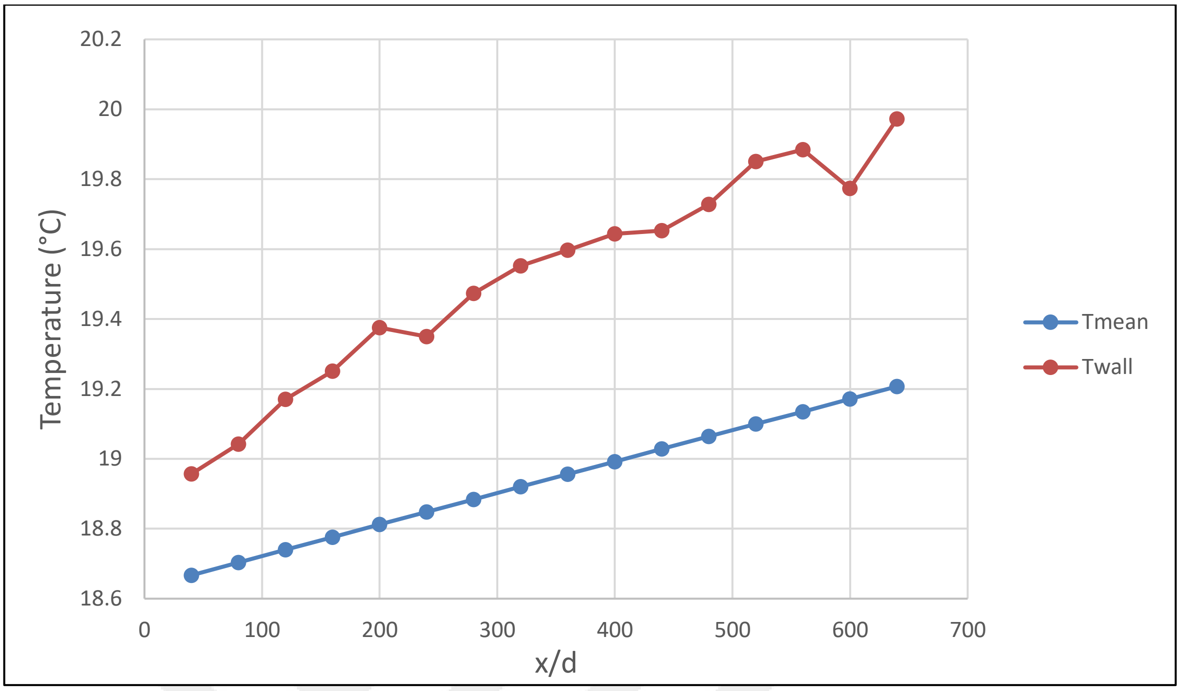

Figure 4.2. Wall temperature and mean temperature comparison for vertically downward configuration for Reynolds at the tube inlet 1943 with 3.5 kW/m^2 heat flux

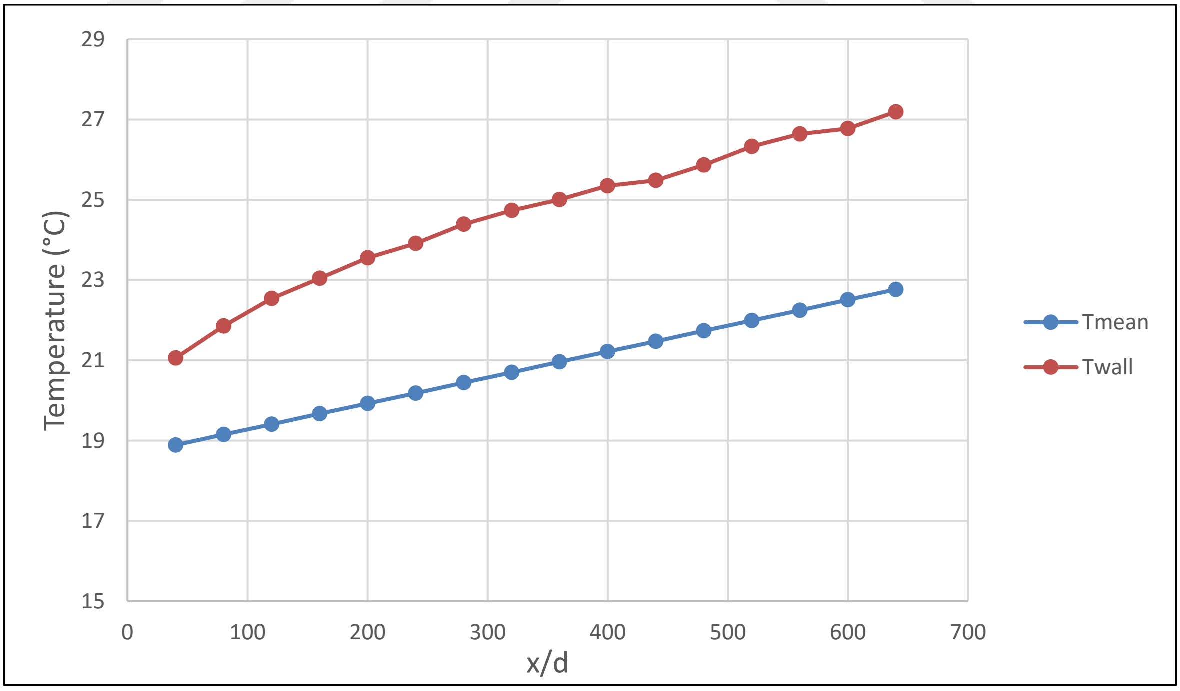

Figure 4.3. Wall temperature and mean temperature comparison for vertically downward configuration for Reynolds at the tube inlet 1943 with 26.8 kW/m^2 heat flux

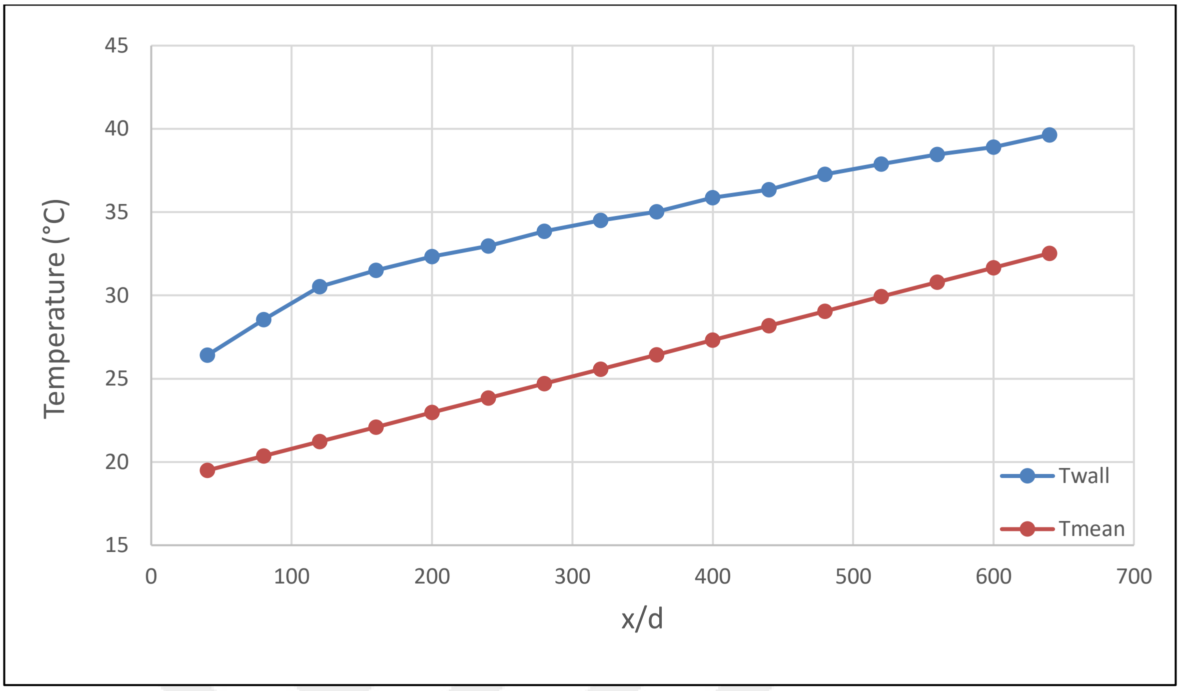

Figure 4.4. Wall temperature and mean temperature comparison for vertically downward configuration for Reynolds at the tube inlet 1943 with 87 kW/m^2 heat flux

The Nusselt number converged to approximately 4.36, as the conventional literature suggested at low heat fluxes. The result of the experiment under the 3.5 kW/m^2 heat flux boundary condition is shown in Figure 4.5. Fluctuations in the figure were observed due to a slight temperature difference between the mean and wall temperature.

Increasing the heat flux value to 6.8 kW/m^2 (Figure 4.6), 10 kW/m^2 (Figure 4.7), and 13.8 kW/m^2 (Figure 4.8) also increases the difference between the mean and wall temperature. Therefore, From Figure 4.6 to Figure 4.8, It can be observed that the Nusselt number is not changing and converges to the literature value of 4.36.

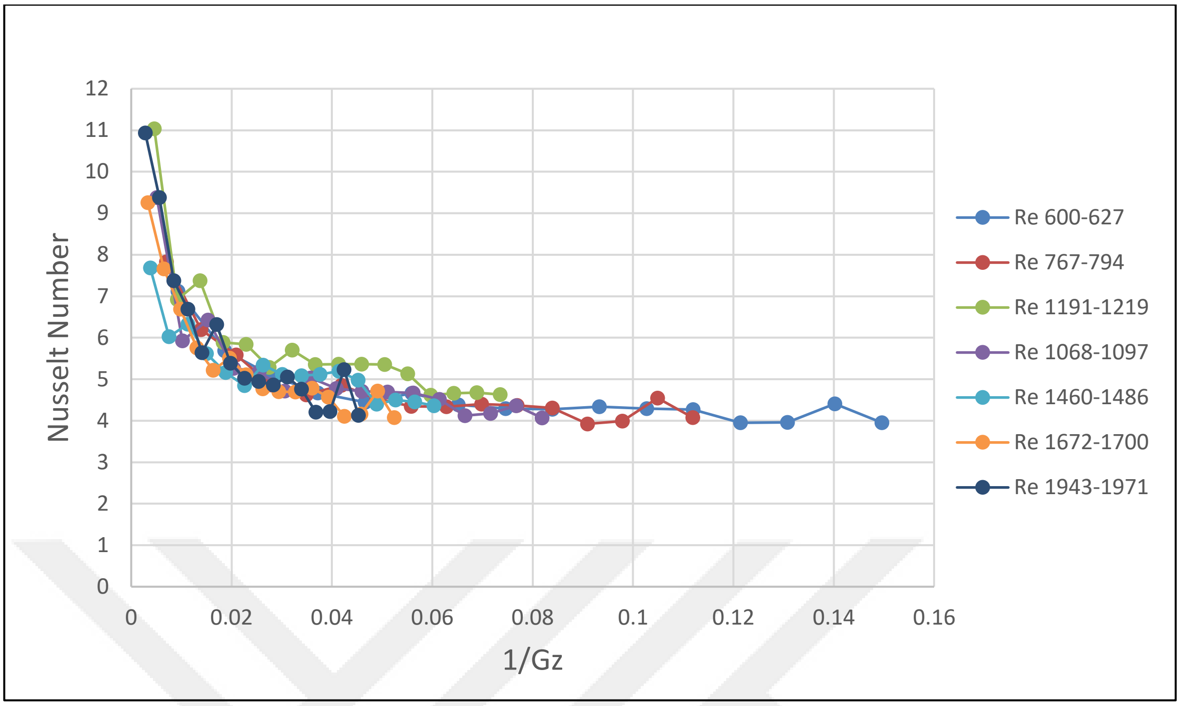

Figure 4.5. Nusselt numbers as a function of inverse Graetz number with the variation of the Reyndols number under the effect of 3.5 kW/m^2 heat flux

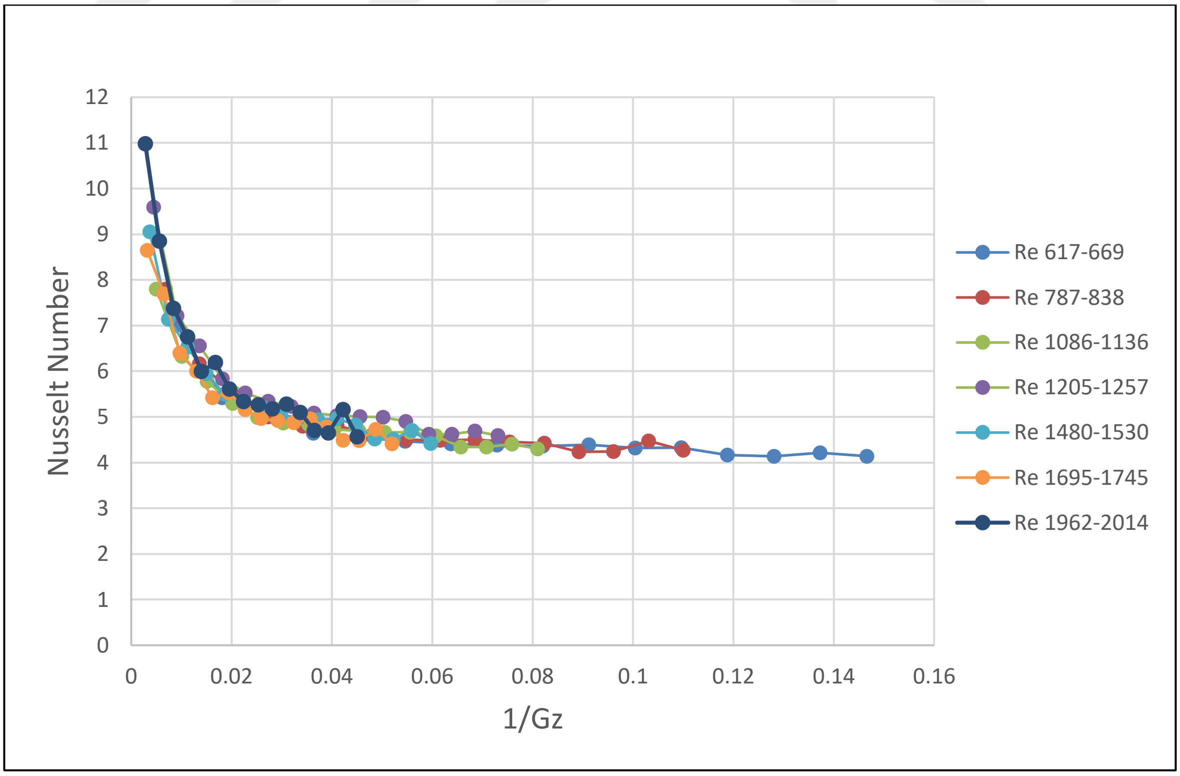

Figure 4.6. Nusselt numbers as a function of inverse Graetz number with the variation of the Reyndols number under the effect of 6.8 kW/m^2 heat flux

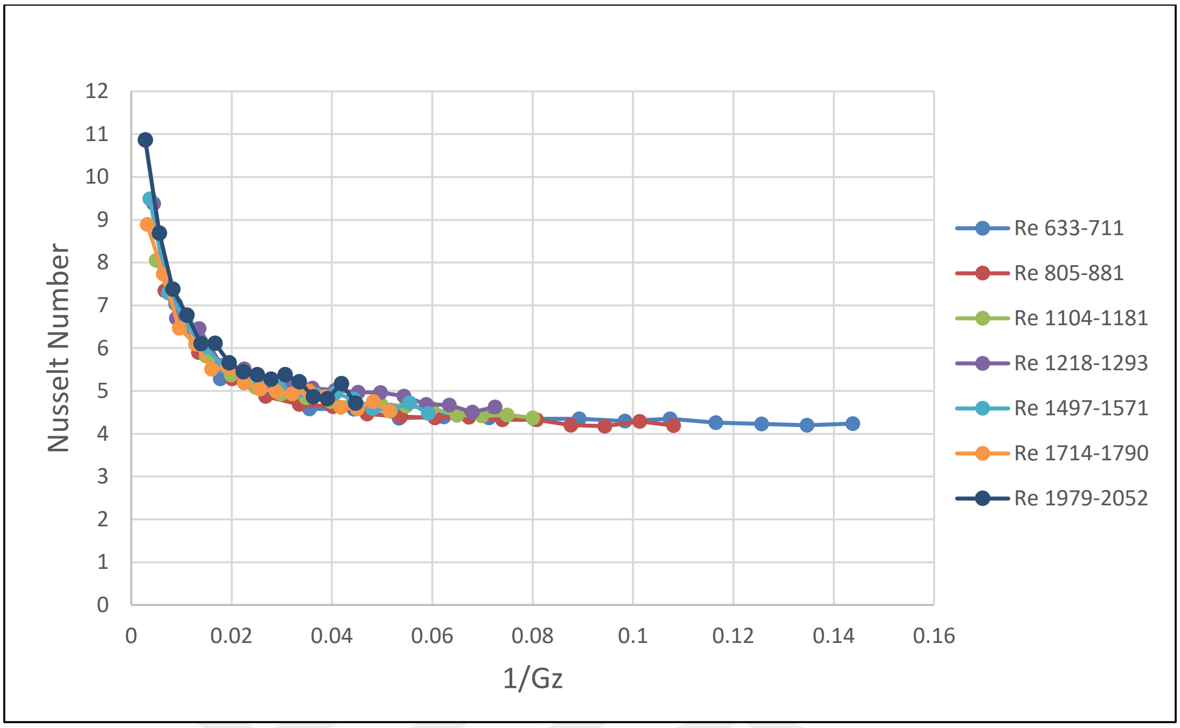

Figure 4.7. Nusselt numbers as a function of inverse Graetz number with the variation of the Reyndols number under the effect of 10 kW/m^2 heat flux

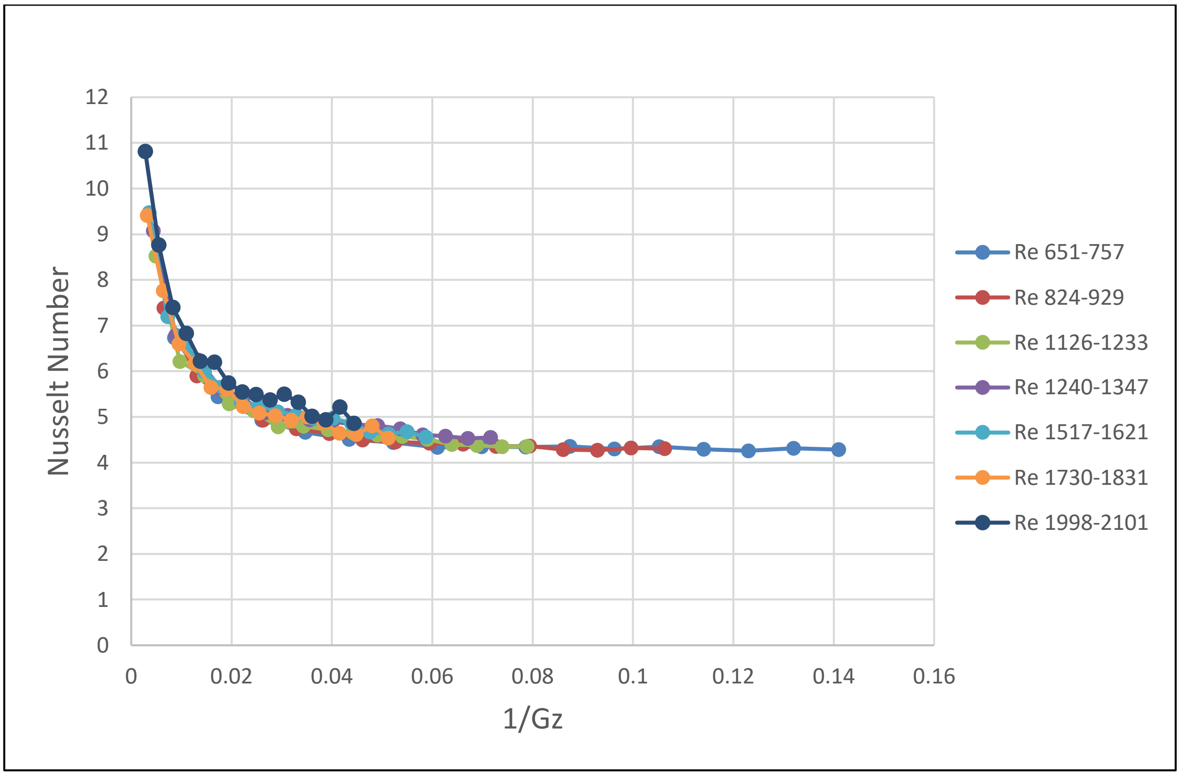

Figure 4.8. Nusselt numbers as a function of inverse Graetz number with the variation of the Reyndols number under the effect of 13.8 kW/m^2 heat flux

A noticeable increase in the Nusselt number first occurs in Figure 4.9, under the effect of 26.8 kW/m^2 heat flux value. This result shows that the effect of natural convection becomes significant, and the Nusselt number increased due to the effect of the mixed convection. As the heat flux increases, the literature value of the Nusselt number, 4.36, becomes invalid. The temperature difference between the tube wall and fluid in this heat flux was 4-5.5 °C.

Increasing heat flux to further values such as 56 kW/m^2 (Figure 4.10) and 87 kW/m^2 (Figure 4.11) dramatically increases the Nusselt number. When the Reynolds number was larger than 2000 at the tube inlet, the heat transfer rate of the vertical flow monotonously increased toward the tube inlet.

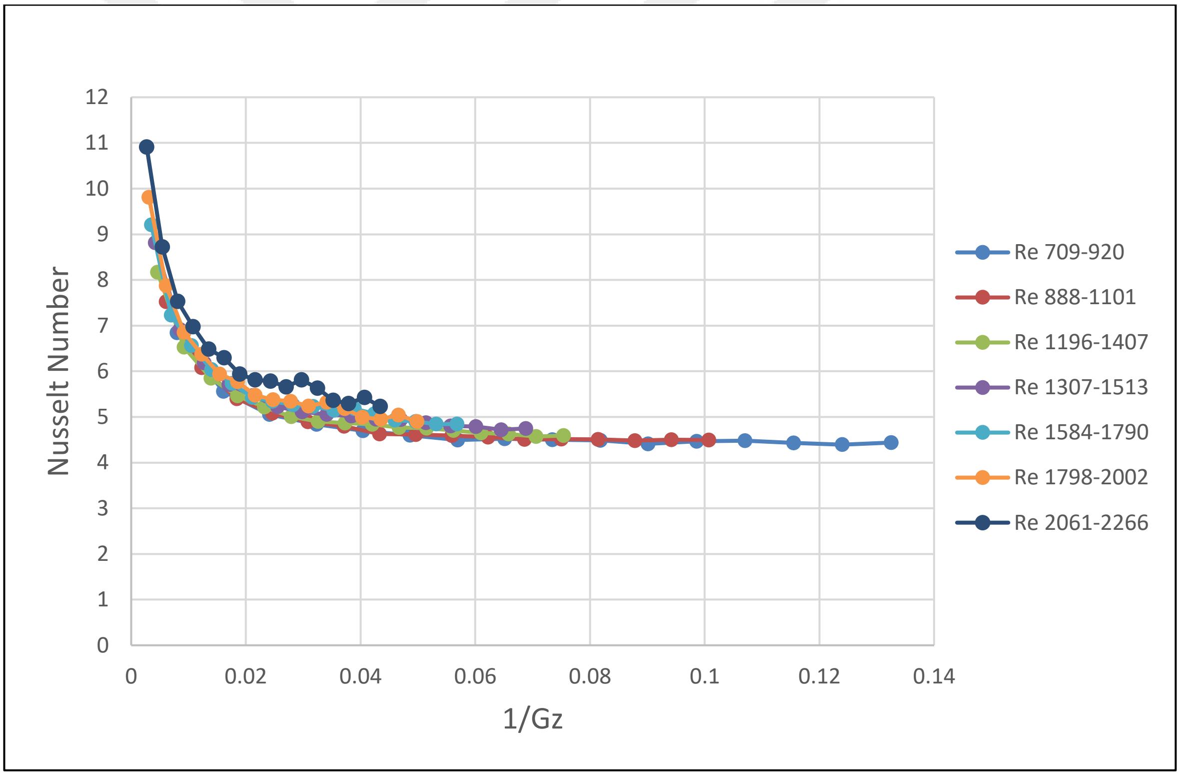

Figure 4.9. Nusselt numbers as a function of inverse Graetz number with the variation of the Reyndols number under the effect of 26.8 kW/m^2 heat flux

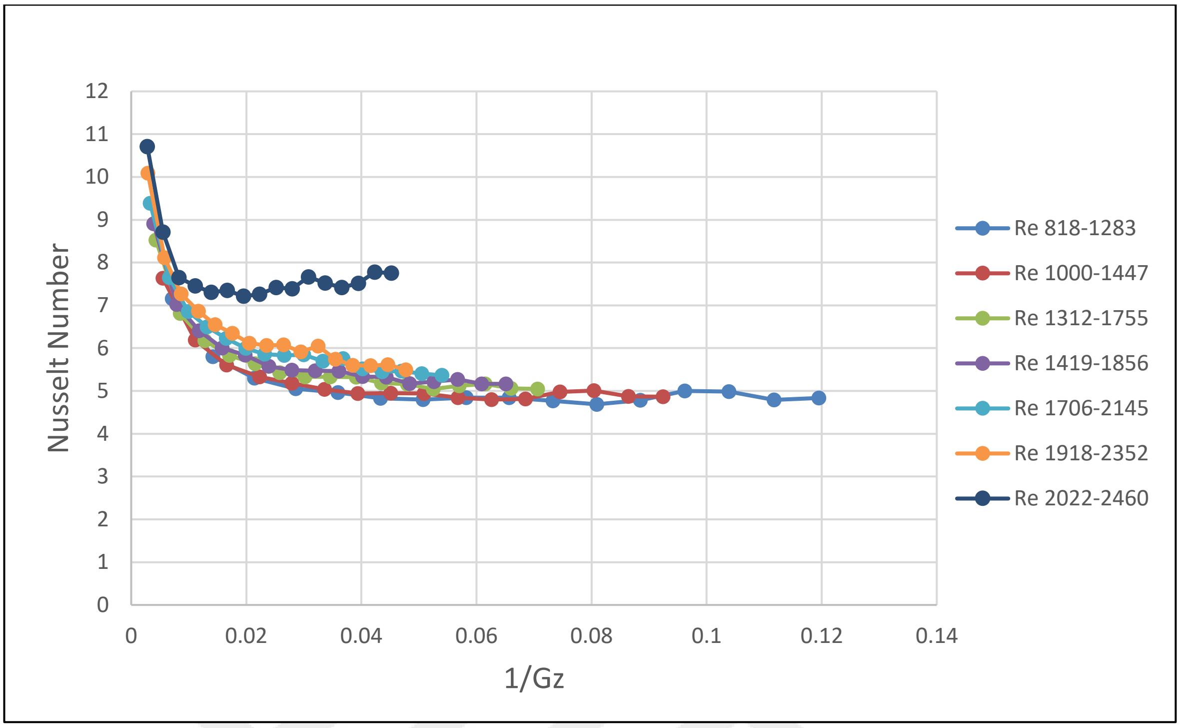

Figure 4.10. Nusselt numbers as a function of inverse Graetz number with the variation of the Reyndols number under the effect of 56 kW/m^2 heat flux

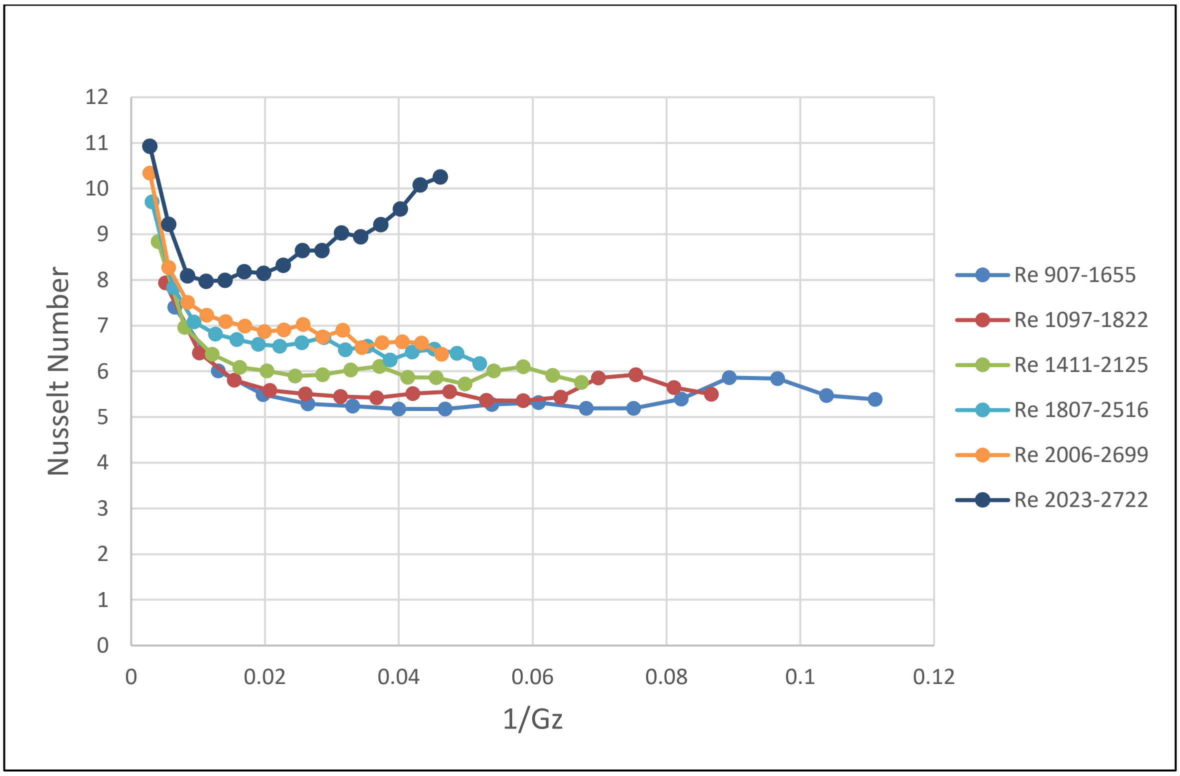

Figure 4.11. Nusselt numbers as a function of inverse Graetz number with the variation of the Reyndols number under the effect of 87 kW/m^2 heat flux

4.2. HORIZONTAL RESULTS

Results represented such as vertical downward experiment results. Reynolds number at tube inlet 690-2192 with heat fluxes between 3.5-87 kW/m^2. Nusselt number was plotted with inverse Graetz number with heat fluxes varying Reynolds numbers at the tube inlet between Figure 4.16 to Figure 4.22.

The blue line represents 0.05 the literature value of the inverse Graetz number and the red line represents the literature value of 4.36 of the Nusselt number in Figure 4.12. As is seen in Figure 4.12, similar to the vertical downward experiments, some of the test results converge to the literature value of 4.36, and this convergence was found to be valid in tests with low heat flux.

Experimental results for horizontal configuration are similar to the vertically downward configuration. As explained in the vertically downward configuration section, due to the slight difference between mean and wall temperature, the most fluctuation was observed under the 3.5 kW/m^2 heat flux boundary condition and increasing the heat flux 3.5 (Fig. 4.16) up to 13.8 kW/m^2 (Fig. 14.19) has a negligible effect on the Nusselt number. For example, the Nusselt number value in the 6.8 kW/m^2 heat flux condition was around 4.43 for Reynolds 915, increasing heat flux to 13.8 kW/m^2 Nusselt number become 4.47. Thus, forced convection effects are still dominant. The effect of the mixed convection was first observed at the heat flux of 26.8 kW/m^2.

Due to the slight difference between the mean and wall temperatures, most uncertainties were observed in the 3.5 kW/m^2 heat flux. And temperature differences are represented in Figures 4.13 to 4.15. The mean and the wall temperature differences in Figures 4.13 to 4.15 were approximately 0.6, 5, and 10 °C, respectively.

Temperature values were not the same at every thermocouple location on the microtube. Since the Reynolds number depends on temperature, the Reynolds number value changes along the microtube. Table 4.2. demonstrate these changes for every heat flux interval. As expected, the most significant increase along the microtube was observed under the 87 kW/m^2 heat flux boundary condition.

Table 4.2. Variation of Reynolds number at different currents along the pipe in the horizontal configuration

Reynolds number at the tube inlet	3.5 [kW/m²]	6.8 [kW/m²]	10 [kW/m²]	13.8 [kW/m²]	26.8 [kW/m²]	55.7 [kW/m²]	87 [kW/m²]
690	690-718	710-763	729-809	758-891	781-955	813-1266	-
915	915-941	933-985	947-1021	963-1066	1020-1228	1134-1574	1208-1922
1140	1140-1165	1156-1209	1170-1246	1187-1292	1246-1454	1347-1785	1434-2147
1285	1285-1312	1289-1339	1298-1371	1309-1416	1354-1563	1426-1869	1501-2202
1467	1467-1495	1490-1542	1506-1580	1525-1628	1593-1797	1706-2138	1802-2489
1645	1645-1666	1659-1709	1674-1745	1697-1800	1764-1967	1883-2315	1977-2664
1871	1871-1895	1885-1935	1902-1977	1919-2020	1987-2190	2100-2530	2192-2876

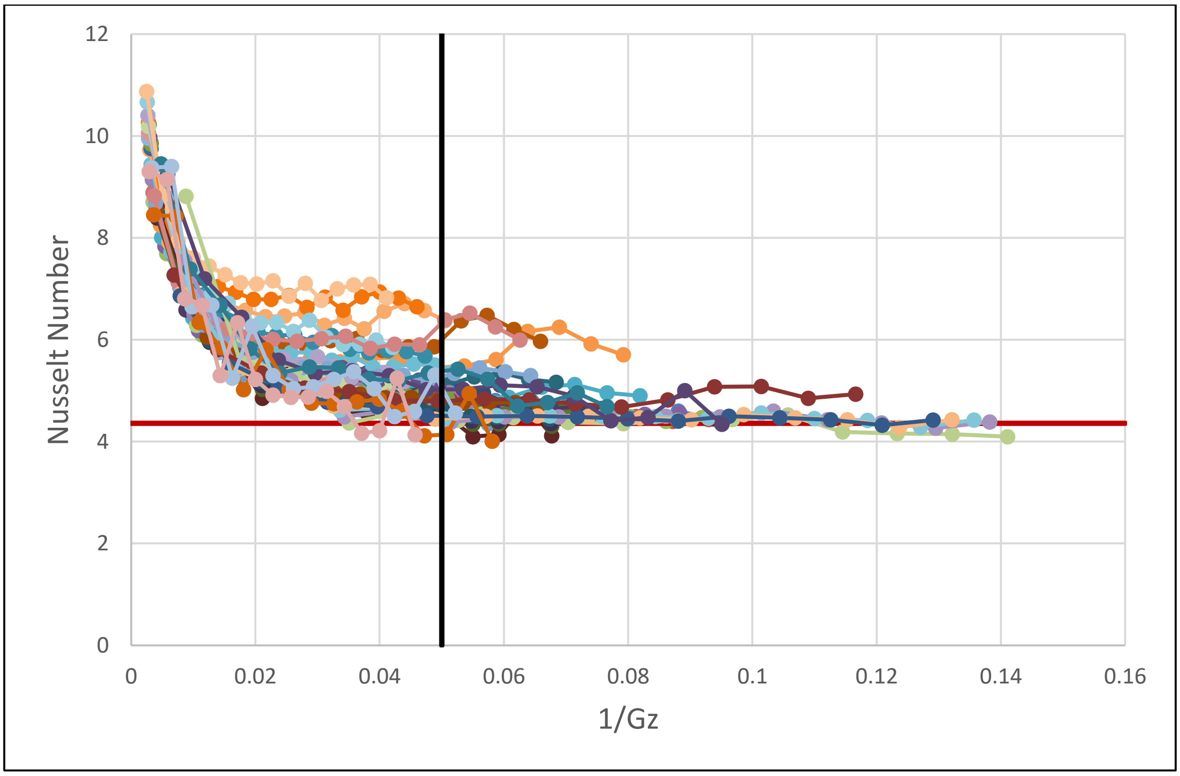

Figure 4.12. Horizontal experiment results in heat fluxes of 3.5, 6.8, 10, 13.8, 26.8, 56, and 87 kW/m^2.

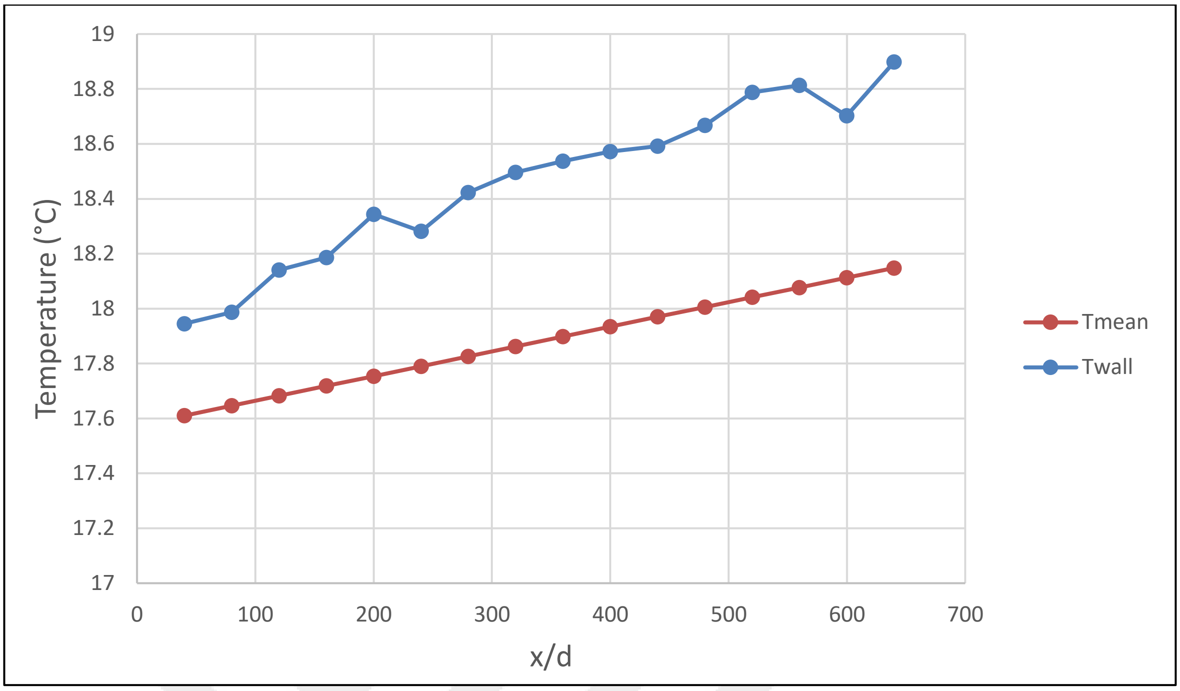

Figure 4.13. Wall temperature and mean temperature comparison for horizontal configuration for Reynolds number at the tube inlet 1871 with 3.5 kW/m^2 heat flux

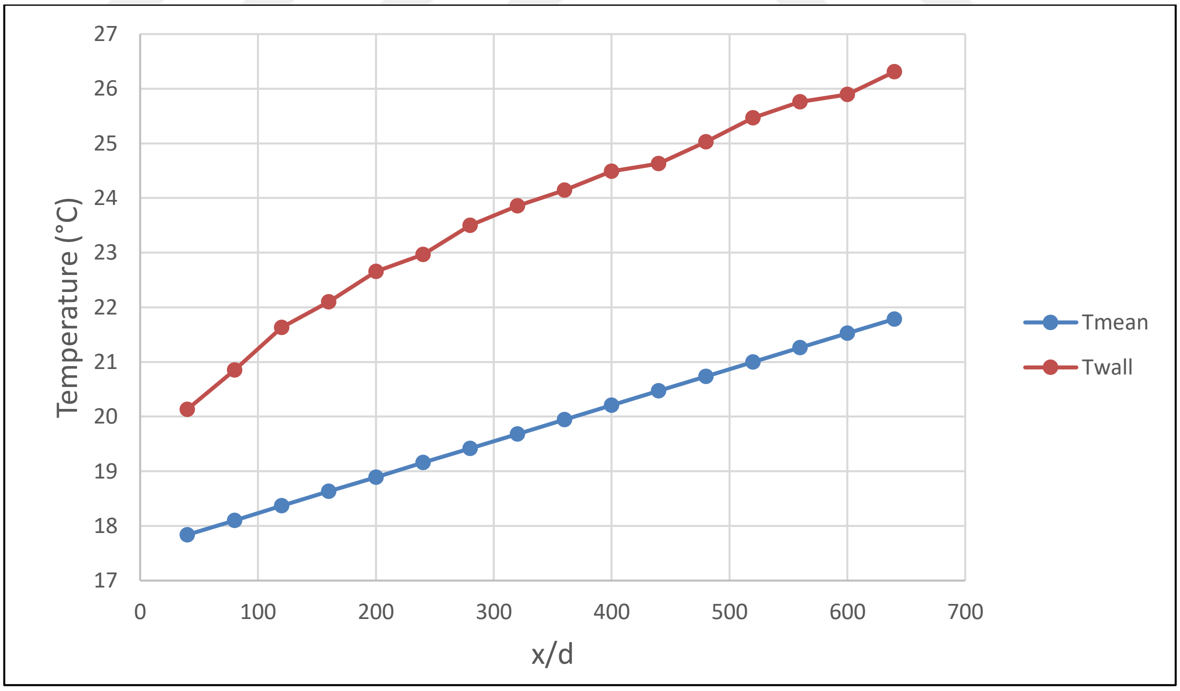

Figure 4.14. Wall temperature and mean temperature comparison for horizontal configuration for Reynolds number at the tube inlet 1987 with 26.8 kW/m^2 heat flux

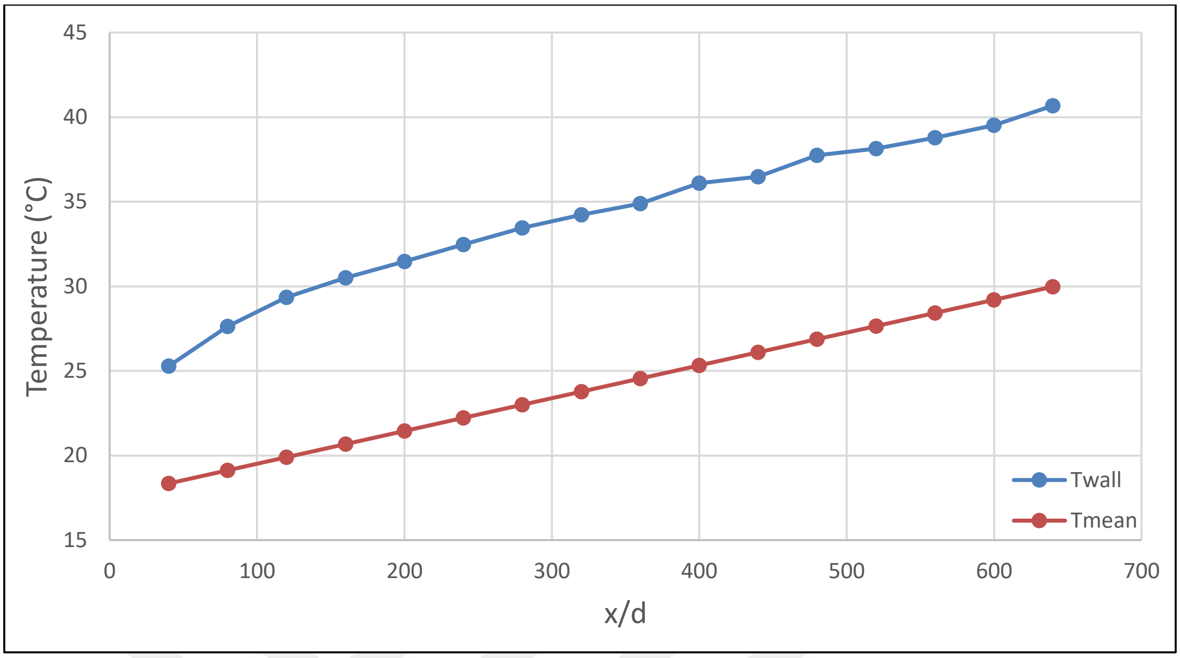

Figure 4.15. Wall temperature and mean temperature comparison for horizontal configuration for Reynolds number at the tube inlet 2192 with 87 kW/m^2 heat flux

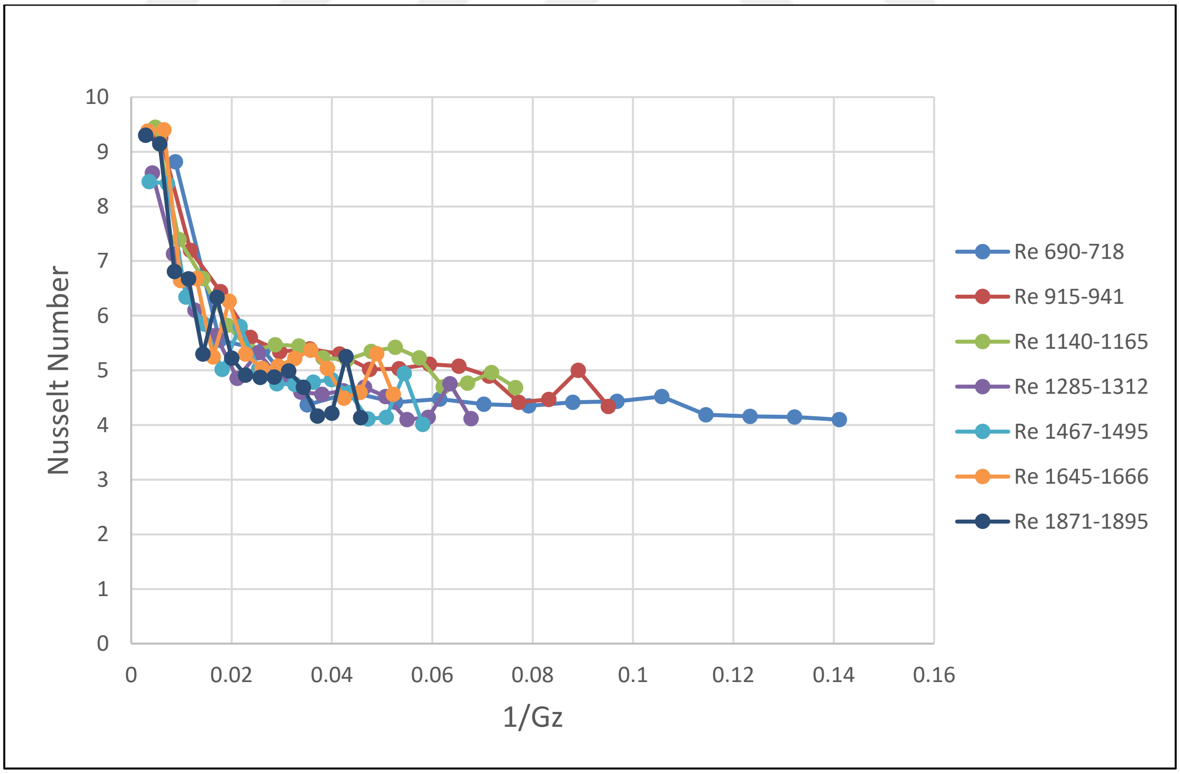

Figure 4.16. Nusselt numbers as a function of inverse Graetz number with the variation of the Reyndols number under the effect of 3.5 kW/m^2 heat flux

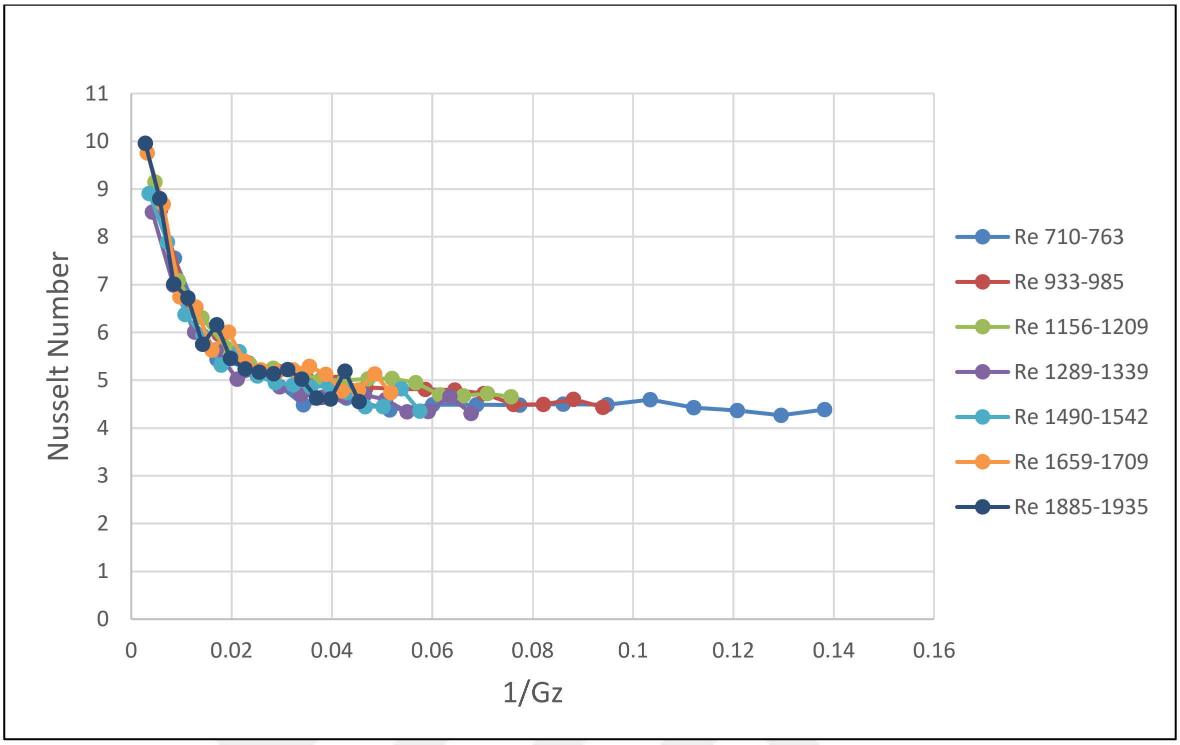

Figure 4.17. Nusselt numbers as a function of inverse Graetz number with the variation of the Reyndols number under the effect of 6.8 kW/m^2 heat flux

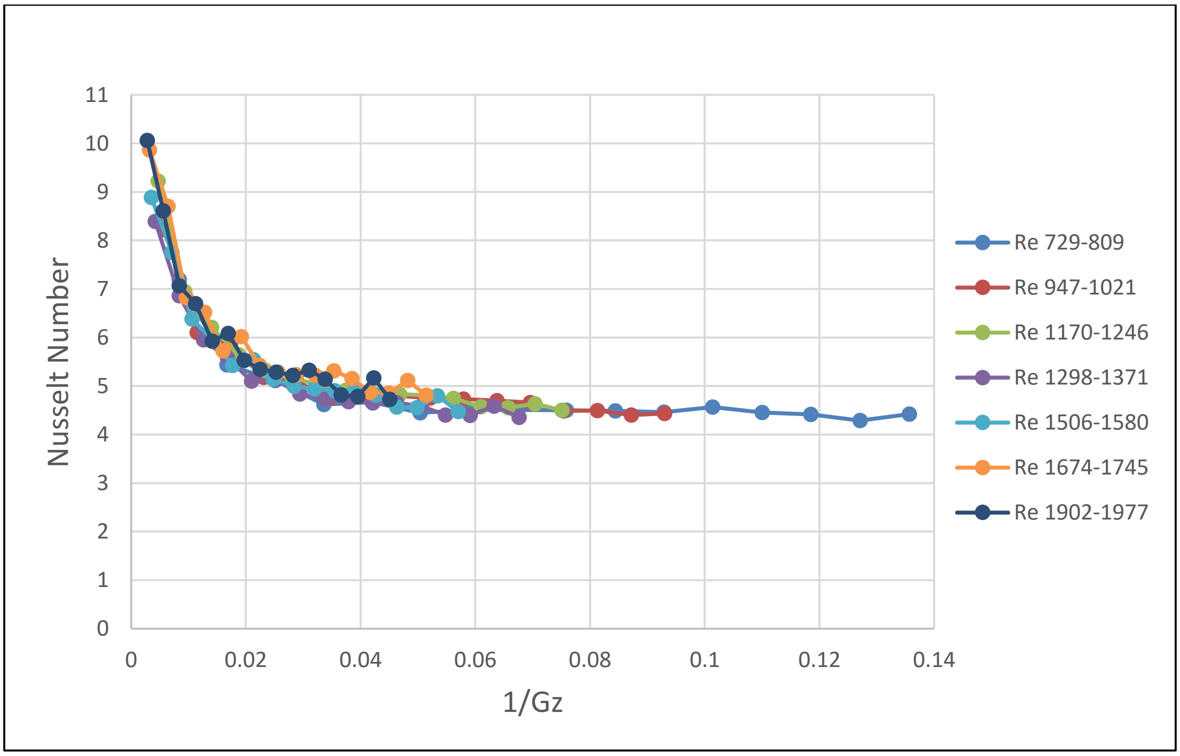

Figure 4.18. Nusselt numbers as a function of inverse Graetz number with the variation of the Reyndols number under the effect of 10 kW/m^2 heat flux

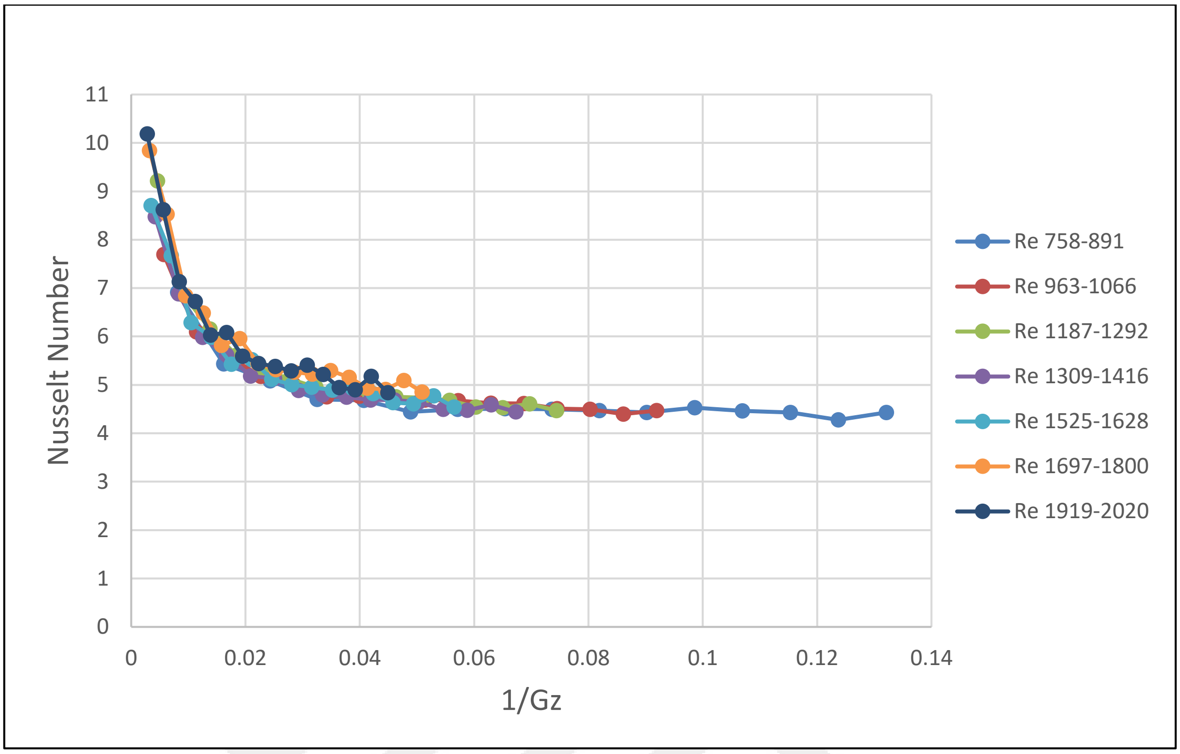

Figure 4.19. Nusselt numbers as a function of inverse Graetz number with the variation of the Reyndols number under the effect of 13.8 kW/m^2 heat flux

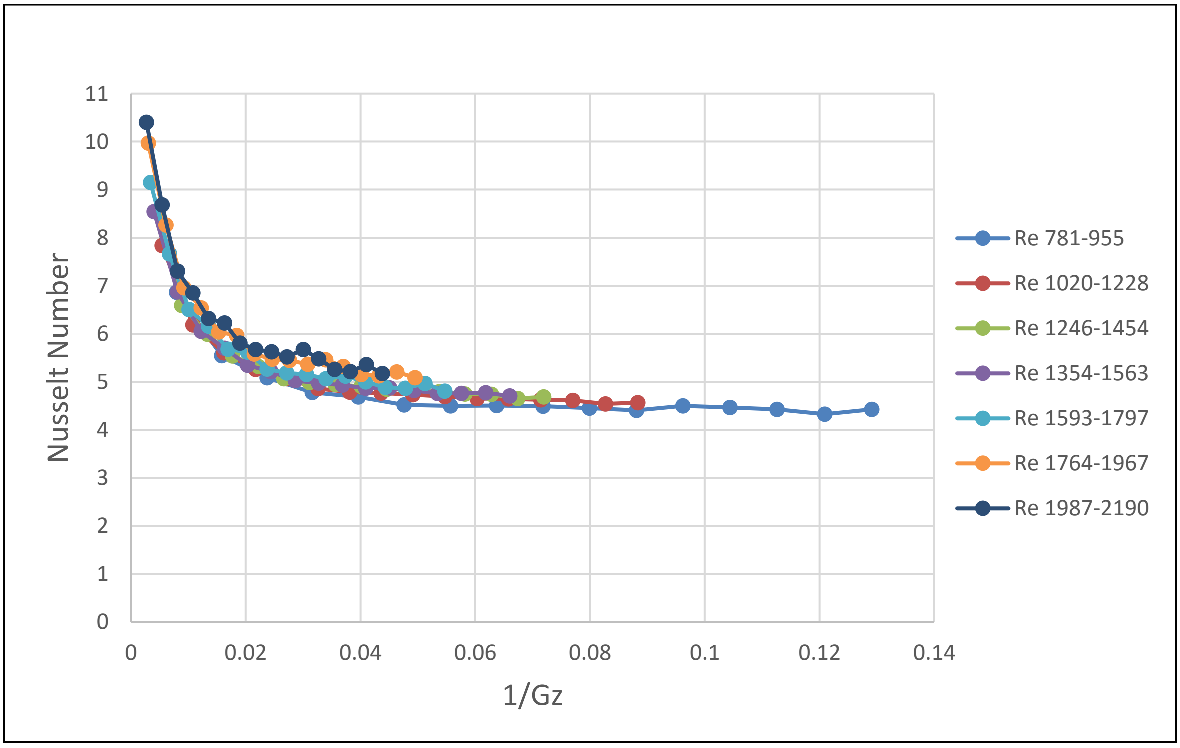

Figure 4.20. Nusselt numbers as a function of inverse Graetz number with the variation of the Reyndols number under the effect of 26.9 kW/m^2 heat flux

As the heat flux increased to greater than 26 kW/m^2, the Nusselt number started deviating far above 4.36. Adjusting heat flux to higher heat values like 56 and 87 kW/m^2 shows a more significant increase in the Nusselt number. However, there was no rapid increase in the heat transfer rate as in the vertical configuration. This result shows that when the Reynolds number at the tube inlet is near 2000, the vertical configuration could be more efficient regarding the heat transfer rate.

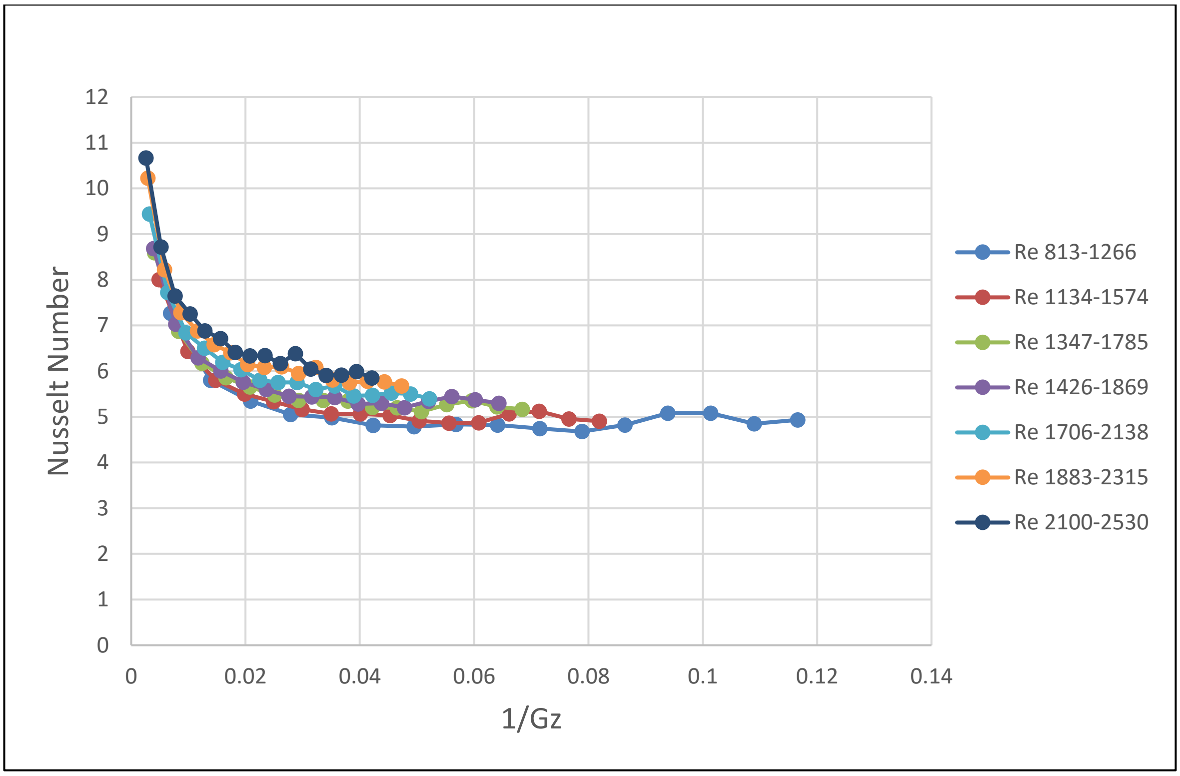

Figure 4.21. Nusselt numbers as a function of inverse Graetz number with the variation of the Reyndols number under the effect of 55.7 kW/m^2 heat flux

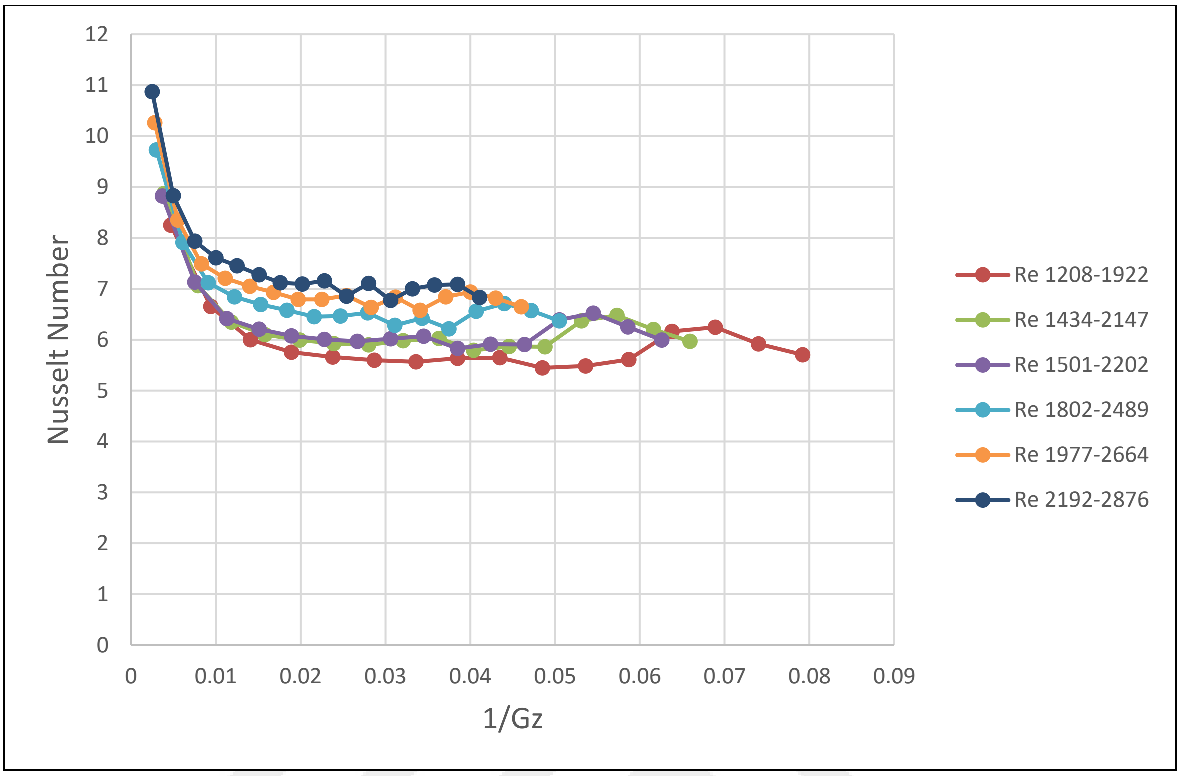

Figure 4.22. Nusselt numbers as a function of inverse Graetz number with the variation of the Reyndols number under the effect of 87 kW/m^2 heat flux

4.3. VERTICAL DOWNWARD AND HORIZONTAL COMPARISON

Experiment results show a negligible difference in the heat transfer rate between vertically downward and horizontal configurations at Reynolds numbers less than 1800 at the tube inlet for all heat fluxes.

Figure 4.23 demonstrated the heat transfer rate of the horizontal and vertical downward configurations under the 3.5 kW/m^2 heat flux boundary condition when the Reynolds numbers at the tube inlet were 1140 and 1191, respectively. There were no significant differences in the heat transfer rates for both configurations. The mean and wall temperature differences were around 0.7 °C when the heat flux was 3.5 kW/m^2. Due to a slight difference, high uncertainty in the Nusselt number was expected in this heat flux. However, experimental results were compatible with the literature value, and the Nusselt number was 6.5% higher than the theoretical value with 22% uncertainty.

Horizontal and vertical experimental results show that the mixed convection effect can be observed when the heat flux value exceeds 26 kW/m^2. The temperature difference between the microtube wall and the fluid in this heat flux is 4-5.5 °C at this heat flux. As the heat flux increased to greater than 26 kW/m^2, the Nusselt number started deviating far above 4.36 due to the effect of mixed convection. A comparison between horizontal and vertical downward configurations with the heat fluxes of 55 kW/m^2 and 87 kW/m^2 is demonstrated in Figure 4.24. Reynolds numbers at the tube inlet were approximately 1700 and 1800 under the 55 kW/m^2 and 87 kW/m^2 boundary conditions, respectively. Heat transfer rates were approximately the same for both configurations. The Nusselt number goes around 6.4 from 5.4 when the heat flux changes from 55 kW/m^2 to 87 kW/m^2 due to mixed convection.

Figure 4.25 shows the difference between vertically downward and horizontal configuration for the Reynolds number at the tube inlet 2192 and 2023 with a heat flux of 87 kW/m^2, respectively. When the Reynolds number was larger than 2000 at the tube inlet, the Nusselt number of vertically downward flow became greater than horizontal flow. Flow in the horizontal configuration became thermally developed. However, the heat transfer rate in the vertically downward configuration increases along with the tube.

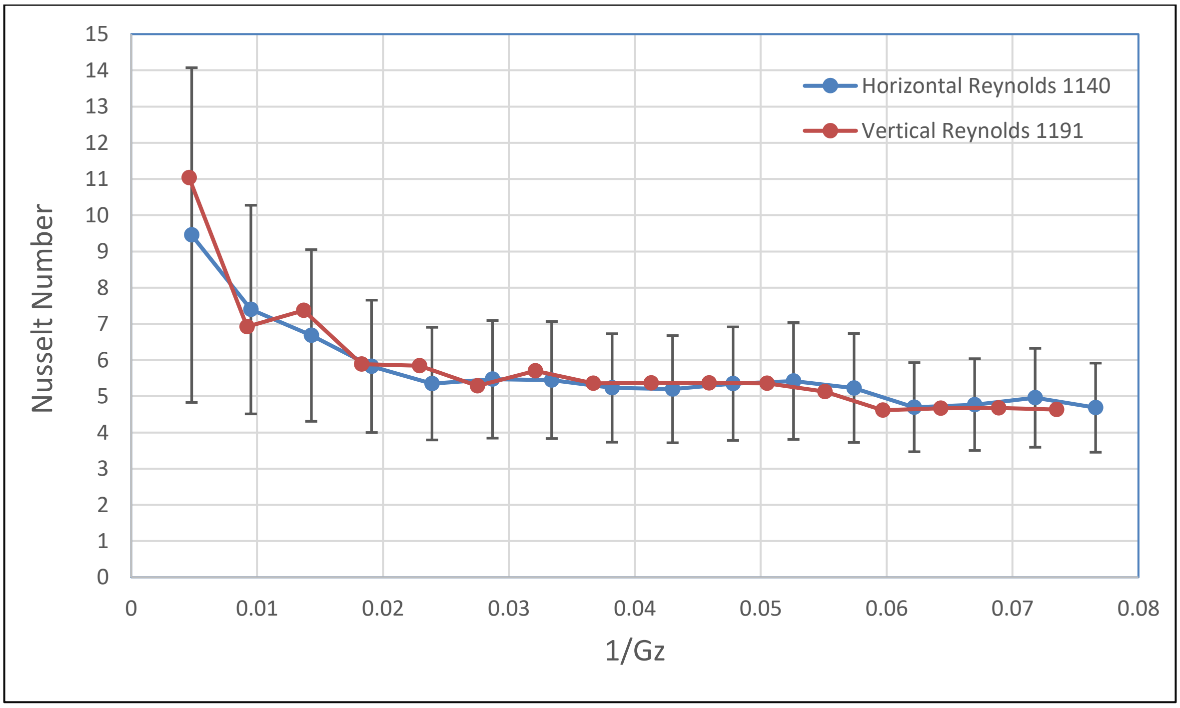

Figure 4.23. Heat transfer rate comparison of Reynolds number at the tube inlet 1140 in the horizontal configuration and 1191 in the vertically downward configuration under the effect of 3.5 kW/m^2 heat flux boundary condition

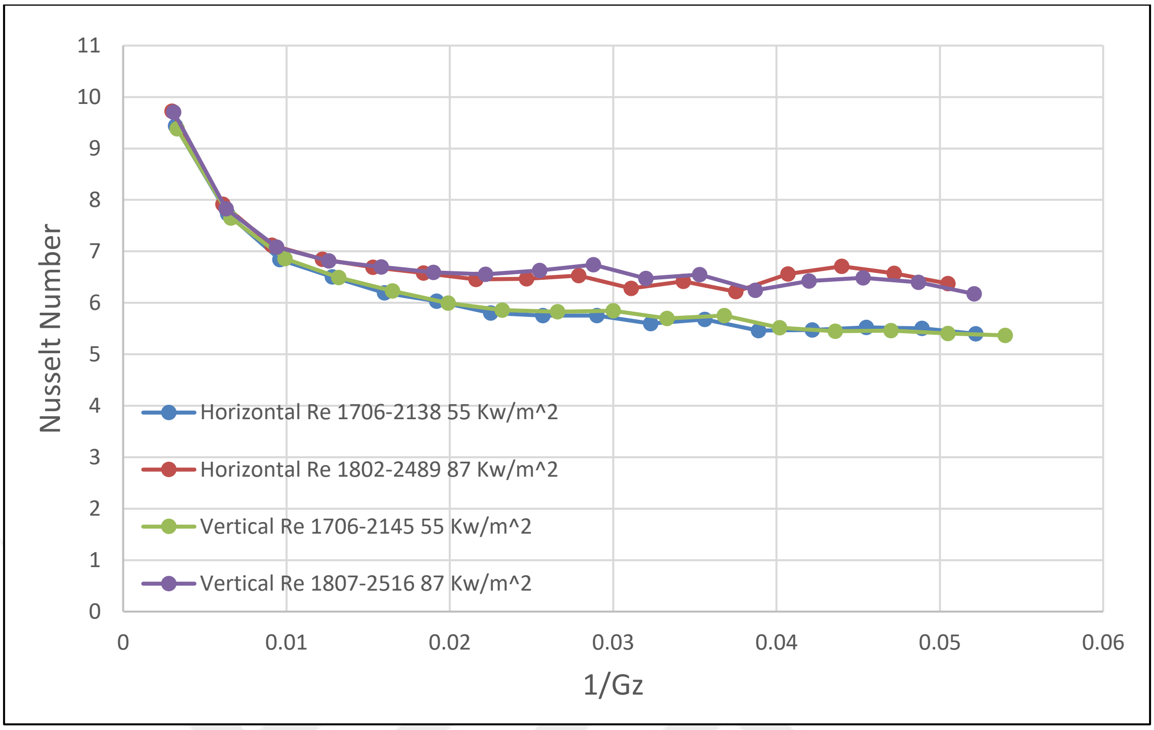

Figure 4.24. Heat transfer rate comparison of Reynolds number at the tube inlet 1706 and 1802 for the horizontal configuration and 1706 and 1807 for the vertical configuration under the effects of 55 kW/m^2 and 87 kW/m^2 heat flux boundary condition

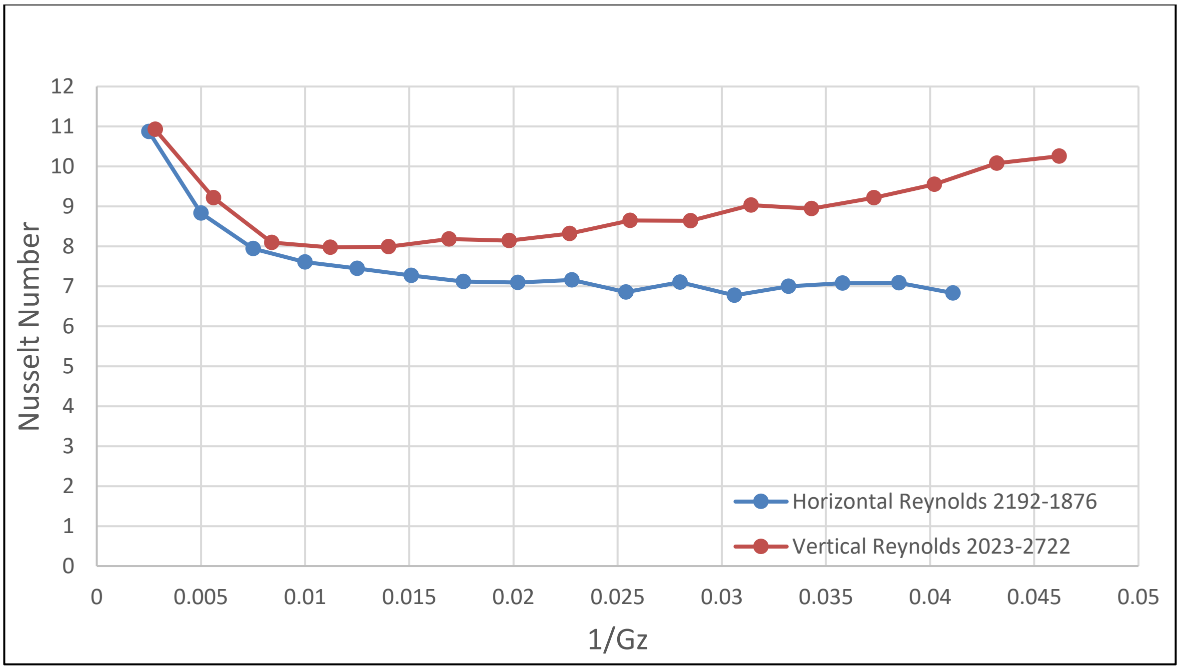

Figure 4.25. Heat transfer rate comparison of Reynolds number at the tube inlet 2192 in the horizontal configuration and 2023 in the vertically downward configuration under the effect of 87 kW/m^2 heat flux boundary condition

5. CONCLUSION

Convection heat transfer of vertically downward and horizontal flows was experimentally studied using a microtube, 0.501 and 1.00 mm in inner and outer diameters, respectively, and 398 mm in length. Tests were conducted with constant heat flux boundary conditions in a vacuum chamber in order to decrease the heat losses to the environment. The wall temperatures were measured employing 17 T-type thermocouples, each embedded in a small solder cast attached to the microtube. Two extra thermocouples measured the environment temperature inside the vacuum chamber. Reynolds numbers at the tube inlet were between 600 and 2000, with heat fluxes varying from 3.5 to 87 kW/m^2. Nusselt number converged to the range of 4.36 and 4.36 + 8% while the heat flux values varied from 3.5 to 13.8 kW/m^2. In order to observe forced convection, heat flux applied to the microtube must be low. Due to low heat flux, the temperature difference between the mean and microtube wall temperature is also low. Most uncertainties in the data were observed in the 3.5 kW/m^2 heat flux boundary condition due to the low-temperature difference. The mean and wall temperature differences were 0.7 °C at a 3.5 kW/m^2 heat flux. The effect of natural convection became noticeable as the heat flux increased to greater than 26 kW/m^2; Furthermore, the difference between the mean and inner wall temperatures at the heat flux of 26 kW/m^2 varied from 4 to 5 °C, depending on the Reynolds number. After the heat flux of 26 kW/m^2, the Nusselt number started deviating far above 4.36 due to the effect of mixed convection. No difference between vertical and horizontal configurations was observed in heat transfer rate at Reynolds numbers less than 1800 at the tube inlet for all heat fluxes. However, when the Reynolds number was larger than 2000 at the tube inlet, the Nusselt number of vertically downward flow was greater than that of horizontal flow. Furthermore, at the high Reynolds number, the heat transfer rate of the vertical flow monotonously increased toward the tube inlet while the horizontal flow appeared thermally fully developed.

6. REFERENCES

1. Meyer JP, Everts M. Single-phase mixed convection of developing and fully developed flow in smooth horizontal circular tubes in the laminar and transitional flow regimes. *International Journal of Heat and Mass Transfer*. 2018;117:1251-73.

2. Celata GP, Cumo M, Marconi V, McPhail SJ, Zummo G. Microtube liquid single-phase heat transfer in laminar flow. *International Journal of Heat and Mass Transfer*. 2006;49:3538-46.

3. Öztabak E, Gökkaya O, Ahn H. A novel method of measuring microtube wall temperatures by thermocouples to investigate sCO2 flows. *Applied Thermal Engineering*. 2022;209:118299.

4. Lin TY, Yang CY. An experimental investigation on forced convection heat transfer performance in micro tubes by the method of liquid crystal thermography. *International Journal of Heat and Mass Transfer*. 2007;50:4736-42.

5. Lelea D, Nishio S, Takano K. The experimental research on microtube heat transfer and fluid flow of distilled water. *International Journal of Heat and Mass Transfer*. 2004;47(12-13):2817-30.

6. Yang CY, Lin TY. Heat transfer characteristics of water flow in microtubes. *Experimental Thermal and Fluid Science*. 2007;32(2):432-9.

7. Li Z, He YL, Tang GH, Tao WQ. Experimental and numerical studies of liquid flow and heat transfer in microtubes. *International Journal of Heat and Mass Transfer*. 2007;50(17-18):3447-60.

8. Baek S, Radebaugh R, Bradley PE. A new method for heat transfer coefficient measurements of single-phase fluids during laminar flow in microchannels. *International Journal of Heat and Mass Transfer*. 2020;157:119891.

9. Everts M, Meyer JP. Flow regime maps for smooth horizontal tubes at a constant heat flux. *International Journal of Heat and Mass Transfer*. 2018;117:1274-90.

10. Ghajar AJ, Tang CC. Heat transfer measurements, flow pattern maps, and flow visualization for non-boiling two-phase flow in horizontal and slightly inclined pipe. *Heat Transfer Engineering*. 2007;28(6):525-40.

11. Barozzi GS, Zanchini E, Mariotti M. Experimental investigation of combined forced and free convection in horizontal and inclined tubes. *Meccanica*. 1985;20(1):18-27.

12. Rosa P, Karayiannis TG, Collins MW. Single-phase heat transfer in microchannels: The importance of scaling effects. *Applied Thermal Engineering*. 2009;29(17-18):3447–68.

13. Maranzana G, Perry I, Maillet D. Mini- and micro-channels: Influence of axial conduction in the walls. *International Journal of Heat and Mass Transfer*. 2004;47(17-18):3993-4004.

14. Mala M, Li D. Flow characteristics of water in microtubes. *International Journal of Heat and Fluid Flow*. 1999;20:142-48